Spring 2017

Biodegradable capacitive pressure sensor toward temporary implants for intervertebral pressure monitoring

Devdatt Chattopadhyay

Department:

BIODEGRADABLE CAPACITIVE PRESSURE SENSOR TOWARD TEMPORARY IMPLANTS FOR INTERVERTEBRAL PRESSURE MONITORING

by

DEVDATT CHATTOPADHYAY

A THESIS

Presented to the Faculty of the Graduate School of the

MISSOURI UNIVERSITY OF SCIENCE AND TECHNOLOGY

In Partial Fulfillment of the Requirements for the Degree

MASTER OF SCIENCE IN ELECTRICAL ENGINEERING

2017

Approved by

Dr. Chang-Soo Kim, Advisor

Dr. Cheng-Hsiao Wu

Dr. Minsu Choi

ABSTRACT

The objective of this thesis is to demonstrate a new class of implantable biomedical device, based on biodegradable borate glass as the substrate material that can be potentially used to monitor the intervertebral pressure in the lumbar region of the human body. Two major types of implantable biomedical devices include the permanent prosthetic devices such as pacemakers and the temporary implants for short-term intervention and monitoring. Unless surgically removed after their intended operation, the temporary implants are left inside the body causing electromagnetic issues, latent complications and various biomechanical safety concerns. In order to address this issue, a new device concept is developed that can be biodegraded inside the body without producing any adverse effects after their operational lifetime.

A series of studies are conducted to design and fabricate a biodegradable capacitive pressure sensor towards intervertebral pressure monitoring. The device is characterized over a wide range of pressure in a phosphate buffer solution environment. The capacitive sensor responds to compressive pressure and remains fully functional for a desired lifetime before it is dissolved, thereby validating the proof-of-concept of a biodegradable device. Borate-based biodegradable glass material is successfully used as a novel functional platform to fabricate solid state sensors towards temporary implantation.

ACKNOWLEDGEMENTS

The work in this thesis has been solely possible with the support and guidance of my advisor, Dr. Chang Soo Kim. His direction has been invaluable and will be greatly appreciated. I would also like to take up the opportunity to thank my committee, Dr. Cheng Wu and Dr. Minsu Choi for their constant encouragement and guidance.

I wish to my express sincere thanks to Dr. Delbert E. Day, Dr. Matthew J. O'Keefe for giving access to different lab facilities. I am grateful for all the help from the technical staffs of Material Research Center: Ron Haas, Eric Bohannan, Brian Porter and also administrative staffs: Sissy and Sarah. I'm thankful to my fellow lab mates Md.Shihab Adnan and Dinesh Reddy for their help from time to time.

I am thankful to God for all the opportunities. I wish to express my endless gratitude to my mother Debjani Chatterjee and father Pradip. Kr. Chattopadhyay for their constant moral support, encouragement.

TABLE OF CONTENTS

Page

LIST OF ILLUSTRATIONS

LIST OF TABLES

1. INTRODUCTION

1.1. CONCEPT OF BIODEGRADABLE IMPLANTS

Permanent prosthetic devices such as cardiac pacemakers and nerve stimulators are actively being developed and used for many therapeutic purposes. In contrast, temporary implants are also necessary to be used for short term medical intervention and monitoring. After their intended operation, these devices are left behind inside the body. Examples of these can be medical RFID tags which are used to identify patient's clinical data. If these tags are not removed, these may be misused for non-medical purposes, leading to breach of one's privacy [4]. Furthermore, it can also cause severe electromagnetic, latent complications and biomechanical concerns leading to ethical issues. Therefore an additional surgery to remove those devices is required. [1-3].

In order to address these issues, a concept of a new class of devices called biodegradable implants has emerged. These devices remain completely functional during their intended operational lifetime when implanted inside the body. After that it is designed to dissolve and be absorbed within the body without producing any adverse effects. The main advantage of using such devices is that it does not need to be removed from the body by additional surgery. The operational lifetime of these biodegradable implants can be modified by altering the chemical composition of the constituent materials from which the devices are made. Hence biodegradable implant is an advanced option for temporary medical intervention and monitoring.

This thesis is focused on fabrication and characterization of biodegradable solid-state devices using a biodegradable glass material. This creates a totally new class of

biodegradable implants that can be potentially used to monitor various physiological parameters inside the body. In particular, a biodegradable capacitive pressure sensor for monitoring of intervertebral pressure has been studied.

1.2. BIODEGRADABLE GLASS MATERIAL

Traditionally glass has been used commonly for dielectric packaging and sealing of electronics and MEMS devices. Many methods and parameters have been established in conventional glass wafer bonding techniques such as fusion bonding, adhesive bonding and anodic bonding. Moreover glass exhibits negligible piezoelectric noise, little dielectric ageing which makes it an excellent material for such purposes [5].

Tissue engineering is for repairing and regenerating soft and hard tissues that have been damaged or lost after injury. One viable approach is to use biodegradable glasses for this purpose. This category of glasses when comes in contact with living tissue alters its chemical composition and either becomes a part of tissues or eventually absorbed by the body.

Borate-based biodegradable glasses react faster with the body fluid and degrade faster than other types of glasses such as silicate-based glasses. In course of degradation, they convert to hydroxyapatite (HA) like material and form a firm bond with the neighboring tissues if the glass contains calcium.

Since the rate of degradation of these glasses can be controlled by changing its composition, it enables us to control the operational lifetime of the device when implanted inside the body. Hence, biodegradable glasses can be an excellent platform for design and development of various temporary implantable medical devices.

1.3. BIOMECHANICS OF HUMAN LUMBAR INTERVERTEBRAL REGION

As can be seen in Figure. 1.1., the human vertebral column is divided into five major segments including cervical, thoracic, lumbar, sacral and coccygeal although the latter two vertebrae are fused together. The vertebral column consists of discs, vertebrae, ligaments and muscles.

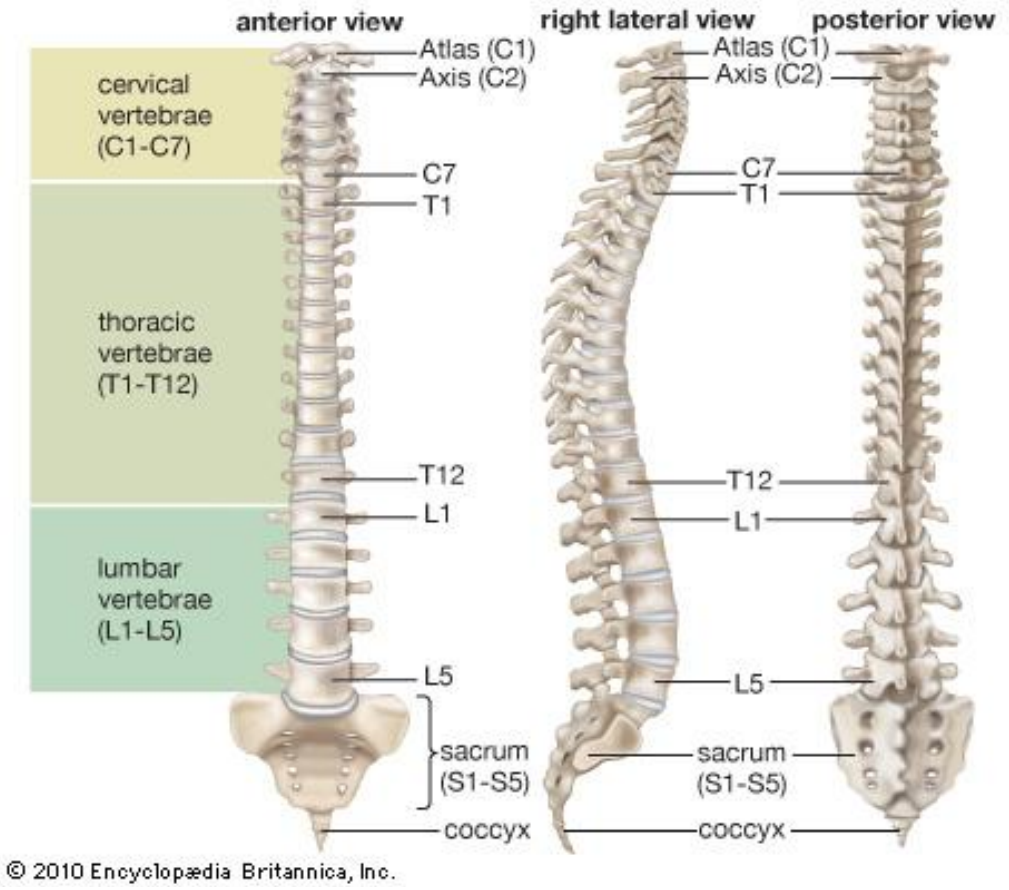

Figure. 1.1. Anterior, right lateral and posterior view of human vertebral column (after [20])

The intervertebral disc shown in Figure. 1.2. is the primary component of a load-bearing element with a unique articular structure. The intervertebral discs absorb and distribute the forces which are applied on the vertebral column. [7]. Located in the

posterior part of the lumbar region of the spine between the cartilaginous end plates, the nucleus pulposus (np) is gelatinous mucoprotein and mucopolysachharide structure surrounded by annulus fibrosis (af) in between vertebral bodies (vb). The outermost fibrous region of annulus fibrosis is posterior longitudinal ligament (pll). The apophyseal joints (aj) protect the disc from bending and shearing. This entire structure is capable of shock absorption and allows bodily movements.

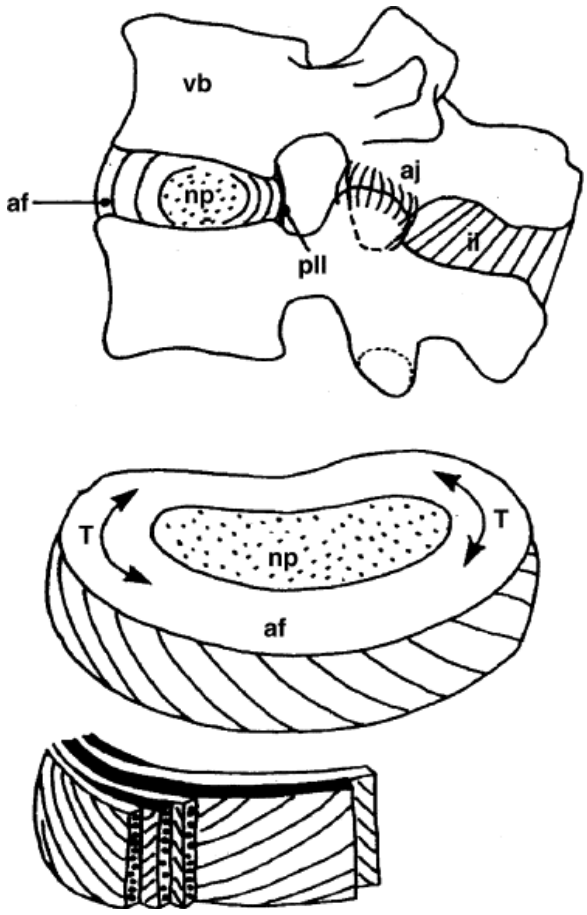

Figure. 1.2. Intervertebral disc showing its various parts (af: annulus fibrosis, aj: apophyseal joint, np: nucleus pulposus, pll: posterior longitudinal ligament, vb: vertebral body) (after [7])

Annually there are approximately nine million MRI examinations of spine are performed due to back pain issues. Back pain arises mainly from physical disruption of intervertebral discs which occurs due to severe mechanical loading with genetic and age-related weakening of the structure [8]. One critical factor in the onset of the lower back pain is the patient's position or posture. It has been seen that the lower back consisting of the lumbar region of the vertebral column is the most affected by back pain of all regions.

Direct measurements of intra-disc pressure were conducted by implanting a pressure transducer in the healthy non-degenerated L4-L5 disc of a male volunteer. It was found that lying supine generates the lowest pressure (0.1 MPa) whereas climbing staircase one at a time generates pressure up to 0.7 MPa [9]. Table 1.1 shows various intradiscal pressure values for different positions. For proper rehabilitation purposes of patients undergoing lower back pain and or spinal-fusion surgeries, practitioners need to precisely monitor the pressure generated within the intervertebral discs during various postures.

Our proposed sensor is designed to measure the pressure generated in the lumbar intervertebral discs when implanted. The range of pressure sensing needed to monitor lumbar pressure is approximately 22 lbs. Assuming the patient will maintain basic body postures and will perform basic movements including supine, sitting, standing, walking and climbing stairs, our proposed pressure sensor has been calibrated up to approximately 40 lbs to maximize the pressure detection range.

Table 1.1. Pressure values generated in intervertebral disc for various body positions and movement (after [9]).

Position	Pressure (MPa)	Equivalent weight (lbs)
Lying supine	0.10	3.19
Relaxed standing	0.50	15.95
Sitting relaxed (without backrest)	0.46	14.67
Walking barefoot	0.53-0.65	16.9-20.73
Climbing stairs (one stair at a time)	0.50-0.70	15.95-22.33

2. DEVICE OPERATION CONCEPT

2.1. CAPACITIVE PRESSURE MEASUREMENT

Capacitive pressure sensing technique had been used for the proposed pressure sensor. This makes use of the impedance or capacitance value in order to determine the pressure generated on the elastomeric insulator by taking into consideration its compressive modulus to ensure repeatability of measurement.

2.1.1. Compressive Modulus. Stress (P) is defined as the force (F) acting on cross-sectional area (A) of an object as shown in eq. (1):

$$P = F/A \qquad (1)$$

Solid objects deform upon application of force, whereas elastic objects tend to return to its original shape when force is removed. For elastic objects, the deformation on application of force is called the strain (ε) and is defined as the ratio of change in dimension to the original dimension as shown in eq. (2):

$$\varepsilon = \Delta d/d \qquad (2)$$

In Figure. 2.1, an external axial compressive force F is applied to an object. The deformation due to the force leads to decrease in thickness of the object to d - Δd and increase in the length to l + Δl, where d, Δd, l and Δl are the original thickness, change in thickness, original width and change in width of the object, respectively.

Elastic modulus is a mechanical property of elastic materials relating stress and strain. For linear elastic materials, the deformation is reversible. The ratio of stress to strain remains constant before reaching a certain point called yield point after which elastic materials show plastic behavior before getting permanent deformed.

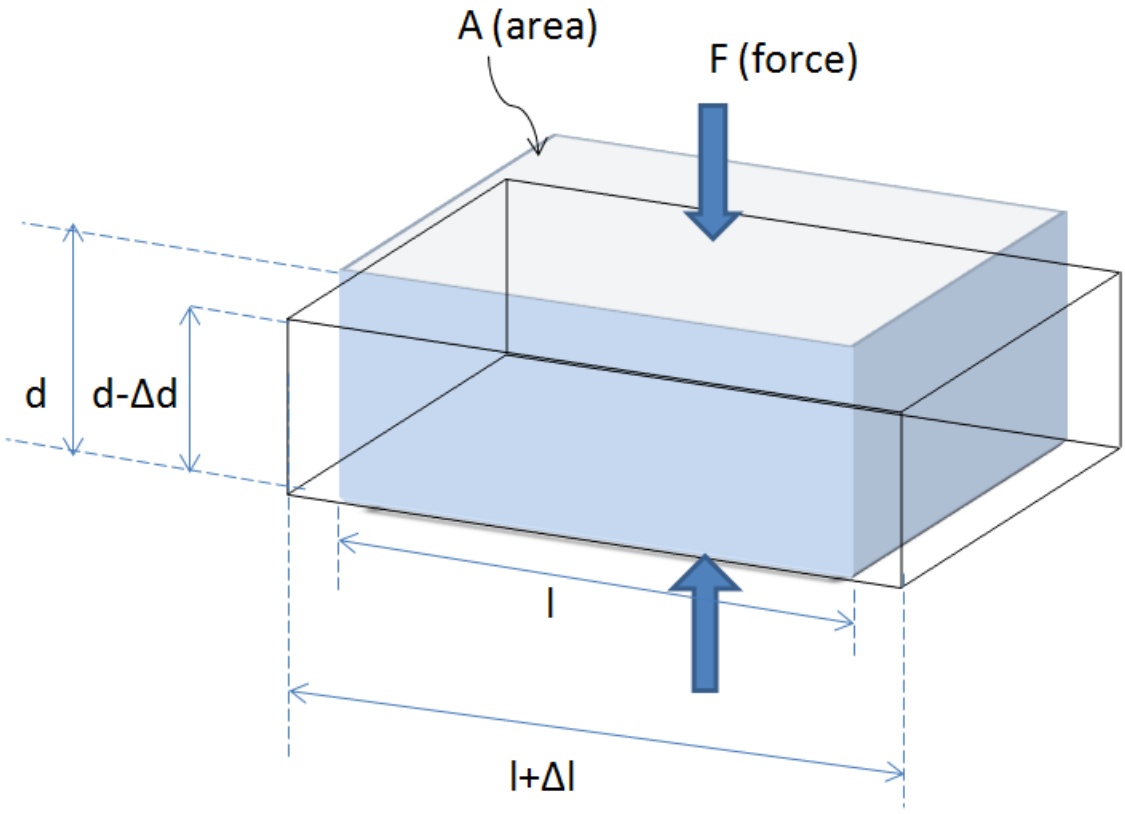

Figure. 2.1. Deformation of object under applied compressive force.

The linear relationship between stress (P) and strain (ε) is a physical manifestation of Hooke's law and it can be written as eq. (3):

$$E = P/\varepsilon \qquad (3)$$

where E is called the Young's modulus. When the applied force is compressive it is called compressive modulus. This value defines how much the material deforms under an applied compressive force until it exhibits plastic deformation. Figure. 2.2. is the stress-strain plot where the slope of the curve indicates the Young's modulus of the material. The linear region indicates that the material still behaves as an elastic material. For the pressure sensor, the sensing elastomer is to be designed to work within the linear region

of the curve to maintain the elasticity of the material to enable continuous monitoring with reproducibility.

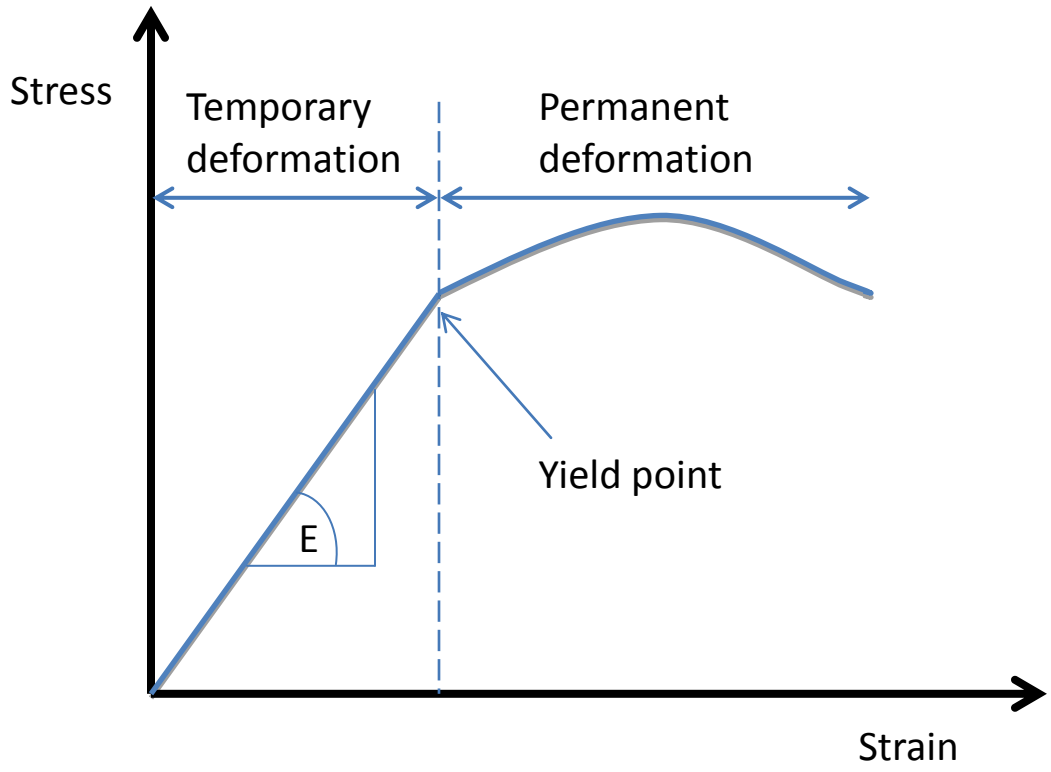

Figure. 2.2. Stress-strain plot of a material.

2.1.2. Capacitive Pressure Sensing. All pressure transducers operate on the mechanism of converting a pressure change into an electrical signal. In this study, the capacitive pressure sensor is characterized by measuring the change in its impedance values with respect to applied pressure. The device structure is based on a parallel plate capacitor where the change in distance between the two electrodes alters the capacitance, thereby exhibiting the impedance of the device. Capacitance of a parallel plate capacitor is given by eq. (4):

$$C = \varepsilon_0 \varepsilon_R A/d \qquad (4)$$

where C, ε_0, ε_R, A and d are capacitance, vacuum permittivity, dielectric constant of the insulator between the electrodes, overlapped area of the two electrodes and distance of separation between two electrodes, respectively.

The impedance of the capacitor is dependent on the frequency of operation, which is given by eq. (5):

$$Z=1/2\pi fC \qquad (5)$$

where f is the frequency of the operation voltage. Combining eq. (3) and (4) leads to:

$$Z = d/2\pi f\varepsilon_0\varepsilon_R A \qquad (6)$$

Eq. (6) indicates that impedance of a capacitor is directly proportional to the distance between two electrodes and also inversely proportional to the frequency.

When an external compressive force is applied to the device, the distance between the electrodes decreases, thereby decreasing the impedance of the device proportionally with the applied force assuming other factors remaining constant. If an elastomeric insulator is used, only temporary deformation of the insulator occurs when compressed by a force. The temporary decrease in thickness of the elastomer exhibits a decrease in impedance within the range of its temporary deformation to enable continuous pressure monitoring with reproducibility.

The best possible method to deliver power and establish communication with the implanted device is wireless connectivity. The wireless connectivity can be realized by designing a L-C resonant circuit. This capability of remote sensing is one of the main advantages of LC sensors. The L-C sensor consisting of the pressure-sensitive capacitor will be implanted inside the body forming a resonant LC tank and a readout coil will be magnetically coupled with the tank to establish connection [21]. The change in pressure

changes the capacitance which in turn changes the resonant frequency. The resonant frequency is detected by the monitoring the impedance of the readout coil. The relation between resonant frequency (f_R), capacitance (C) is given by:

$$f_R = 1/ [2\pi(LC)^{1/2}] \qquad (7)$$

In this thesis, only the working of pressure sensitive capacitor is demonstrated, keeping the wireless approach for future implementation.

2.2. DEVICE OPERATION LIFETIME

Figure. 2.3. shows the prospective functionality of the biodegradable pressure sensor implanted inside the human body and exposed to body fluids. On the surfaces of two identical substrates is a thin film of slow-reaction glass material whereas the major portion of the substrate is based on fast-reaction glass material. The slow-reaction glass portion dissolves in the body fluid during the time frame between stage A and stage B. This time duration is the intended operational lifetime during which the device stays functional after implantation. At the end of this functional time period, the fast reacting glass is exposed and comes in contact with the body fluid. The lifetime of the device can be largely manipulated by changing the elemental composition of the slow-reaction glass. Also altering the thickness of the slow- reaction glass is another option to control the lifetime of the device.

Interval between B to C indicates an unstable and unreliable device operation due to rapid structural disintegration. Sudden failure at stage C is represented by the steep decrease of impedance because the two electrodes come in contact with the conductive body fluid thereby creating a short circuit. The elastomer is the only element which is left

behind after the dissolution. Since it is very thin (in the order of micrometers) with a small volume and bio-inertness in nature, it is expected that the element will not cause any health hazard to the human body even if it stays inside the body.

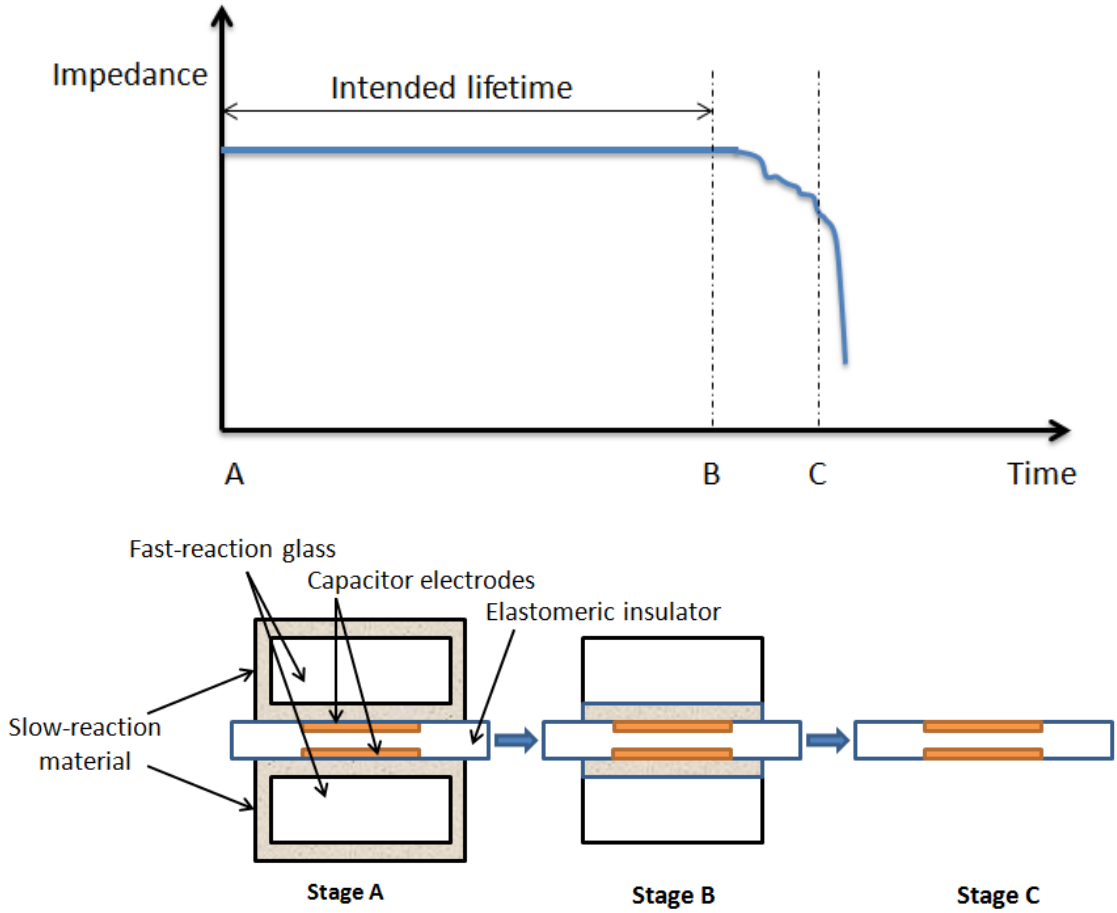

Figure. 2.3. Conceptual diagram of device functionality in terms of its impedance over time.

3. EXPERIMENTALS

3.1. MATERIALS

In this thesis, biodegradable borate glass (99.5 % anhydrous sodium tetra borate $Na_2B_4O_7$, Alfa Aesar) has been used as the main structural material to develop the pressure sensor. On course of its degradation, this glass completely dissolves inside the body leaving no hydroxyapatite residues due to absence of calcium ingredient. The rate of degradation of this borate glasses is higher than that of borate glasses containing silicates [10, 11]. In this proof-of-concept stage, there is no protective slow-reaction material coated on the glass substrate and hence we see a rapid degradation of the device structure. Therefore, this thesis is focused on demonstrating the working of the device structure for a short period of time depicted between stages B to C in Figure. 2.3. The biodegradable glass substrates were prepared manually in form of discs and it is expected that they can be mass-produced industrially in a more refined manner in a later stage of development.

A polydimethyl siloxane (PDMS) elastomer (Sylgard 184, Dow Corning) has been used as the elastic insulator between the electrodes of the capacitor. PDMS commonly known as silicone, is an elastic, inexpensive polymer widely used in various lab-on-chip (LOC) platforms due to its advantages of biocompatibility, elasticity and processability for device fabrication. PDMS sheets can be easily prepared by spin coating processes. PDMS also has an excellent property to bond to itself and also other materials creating water-tight seals. It is known that PDMS retains its bulk elastic property when

the sample has at least 200 µm thickness [12]. This is the proper range of dimension for sensor applications for biomechanical pressure monitoring.

All the dissolution tests performed in this experiment were conducted in phosphate buffer saline (PBS) solution (pH 7.4, Sigma-Aldrich) and the temperature of the solution was kept at 37 ^{o}C using a hot plate and incubator (Heratherm Incubator, Thermo Scientific). This PBS is used to simulate body environment because the osmolarity and ion concentration of this saline solution resemble those of the body fluids.

3.2. DEVICE DESIGN AND FABRICATION

Proper designing and fabrication of the pressure sensor is important to achieve reliable and accurate functionality. The following sections describes the design and fabrication process and parameters used to develop the sensor.

3.2.1. Device Design. The dimensions of the lumbar vertebrae and discs are critical for the design of appropriate pressure sensor for spinal pressure monitoring. Figure. 3.1. depicts a typical upper vertebral width (UVW) or lower vertebral width (LVW) and upper vertebral depth (UVD) or lower vertebral depth (LVD) of vertebral endplates shown by the length ‘a’ and ‘b’ in the cross-sectional view of a lumbar vertebral disc. Table 3.1. shows the mean and standard deviation values of the UVW or LVW and UVD or LVD of L4 and L5 obtained from the study of 126 adults patients. These patients had low back pain and varying degrees of disc degeneration but none had abnormalities or other major spinal pathologies including spondylolisthesis and disc space collapse, etc. The diameter of the sensor device is designed to be 14 mm so that it can be easily placed in the central region of the vertebral body [13].

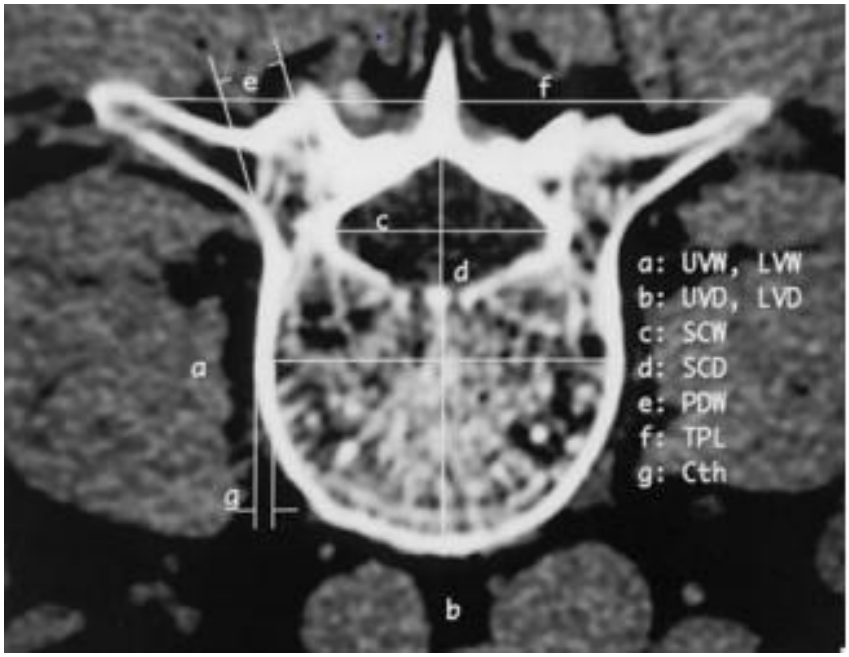

Figure. 3.1. Cross-sectional image of fourth lumbar vertebral body (L4) of 47-year-old male subject (after [13]).

Table 3.1. Mean and standard deviation values of vertebral widths and vertebral depths of L4 vertebral disc (after [13]).

	Mean	Standard Deviation
Upper vertebral width (UVW) or lower vertebral width (LVW)	50.30 mm	0.26 mm
Upper vertebral depth (UVD) or lower vertebral depth (LVD)	34.80 mm	0.44 mm

The dimension of intervertebral disc space geometric is also an important factor to design the thickness of the pressure sensor. The normal lumbar disc space between third - fourth and fourth - fifth lumbar discs were measured by magnetic resonance imaging (MRI) in total 178 adult patients having lower back pain, but no other critical spinal

pathological conditions [14]. Table 3.2. shows the average distance of intervertebral space (from L3 to L5) of the anterior, middle and posterior regions.

Table 3.2. Distance of intervertebral space of 178 adults (after [14]).

	L3-L4	L4-L5
Anterior	9.86 mm	10.83 mm
Middle	9.64 mm	10.05 mm
Posterior	6.78 mm	7.20 mm

Keeping in mind the minimum distance between the discs amongst all these values shown in the table, our proposed pressure sensor is made by using two glass substrates, each with thickness of 2.8 mm making the total thickness of the sensor device approximately 5.6 mm. The thickness of the sensor can be altered anytime depending on the particular use and placement position inside the disc area. Moreover, fabricating too thin glass discs may result in breaking of glass when a strong load is applied. Therefore the thickness chosen for the glass discs is very apt. Although the durability of the glass discs below 2.8 mm thickness have not yet been tested under pressure in this thesis.

The circular electrode with 8 mm diameter is prepared on the center of the glass disc having 14 mm diameter. This allows a 3 mm distance between the edge of the glass substrate and the electrode. The PDMS elastomer used here has a dielectric constant of approximately 2.7 at 100 Hz -100 KHz range. Circular PDMS sheets of diameter 16 mm was used to entirely cover the glass substrate to ensure water-sealing. The thickness of the elastomer was approximately 250 μm to retain its bulk elasticity when the external compressive force is removed. This parallel-plate capacitor structure produces a

capacitance of 7.2 pF at 1 KHz based on eq. 5. without compressive pressure. Hence with each biodegradable glass discs being 14 mm diameter, 2.8 mm thick, circular electrode diameter of 8 mm and PDMS elastomer thickness approximately 250 µm and diameter of 16 mm, the dimension of the final sensor device becomes 16 mm diameter and approximately 5.6 mm thick.

3.2.2. Device Fabrication. Borate glass substrates were prepared by melting 99.5 % anhydrous sodium tetra borate in a platinum crucible at 1000 ^{o}C for 30 minutes. The molten glass was then immediately poured in stainless steel molds having dimensions 14 mm diameter and 30 mm height. The mold was annealed at 450 ^{o}C for 30 minutes and then kept inside melting chamber overnight for slow cooling with the chamber turned off. The glass rods (14 mm diameter and 30 mm long) were then sliced using a circular low-speed saw (Isomet, Buehler) to form glass substrates of approximately 2.8 mm thickness.

The glass discs were then cleaned with acetone and mounted on aluminium holders using a thermoplastic adhesive (Brewer Bond, Brewer Science). They were clamped into the specimen holder and polished using silicon carbide foils (180 µm to 1200 µm grit sizes, Struers) followed by diamond polishing using diamond media (DP spray P, Struers) in the automatic polisher machine (Tegramin 30, Struers). After polishing, the discs were demounted and cleaned ultrasonically in dodecene and then isopropanol each for 15 minutes. It was followed by wiping the discs using microfiber cloth (TX 1009, Alpha Wipe) and then spraying isopropanol on it. Finally it was blown dried using compressed nitrogen gas.

The electrodes of the parallel plate capacitor (8 mm diameter) were prepared with gold layer (120 nm thick) deposited by sputtering using a flash coater (E5400, Bio-Rad). It was patterned using a polymer shadow mask on glass substrate during deposition.

The elastomeric insulator was fabricated using PDMS. It is a two part mixture, where the base and the curing agent are mixed thoroughly in the ratio of 10:1 by weight. It is then degassed using a vacuum chamber for 30 minutes. The degassed mixture was spin coated with a spin coater (WS-400B-6NPP/LITE, Laurell) on circular acrylic sheet (Optix, Plaskolite Inc.) of 8.5 cm diameter and 2 mm thickness. A coating at 400 rpm, 50 rpm^2 acceleration for 30 seconds followed by curing at room temperature for 48 hours. The resulting thickness of the PDMS obtained was approximately 250 µm. It was cut into circular pieces of 16 mm diameter with hollow metal puncher. Prior to bonding, it was ultrasonically cleaned with ethanol for 5 minutes and then dried using compressed air.

One side of the PDMS insulator and one side of the glass disc where the electrode is deposited were treated by oxygen plasma with a reactive ion etcher (PE-200, Plasma System). Then the plasma-treated surfaces of both insulator and glass substrate were made to hold against each other to bond irreversibly. Then the other glass disc and the other surface of the previously bonded insulator were bonded through the same procedure. Figure. 3.2. shows the cross-sectional view of the fabrication process flow.

Coaxial cables were then connected to the trace of the electrodes formed over the side walls of the glass substrates using a silver paste (SEC1233, ResinLab). To give mechanical strength and passivation against solution to this connected portion, an epoxy and encapsulant (JB Weld Epoxy and Dow Corning RTV Silicone) respectively were applied. Figure. 3.3. is the photograph of the final assembled device.

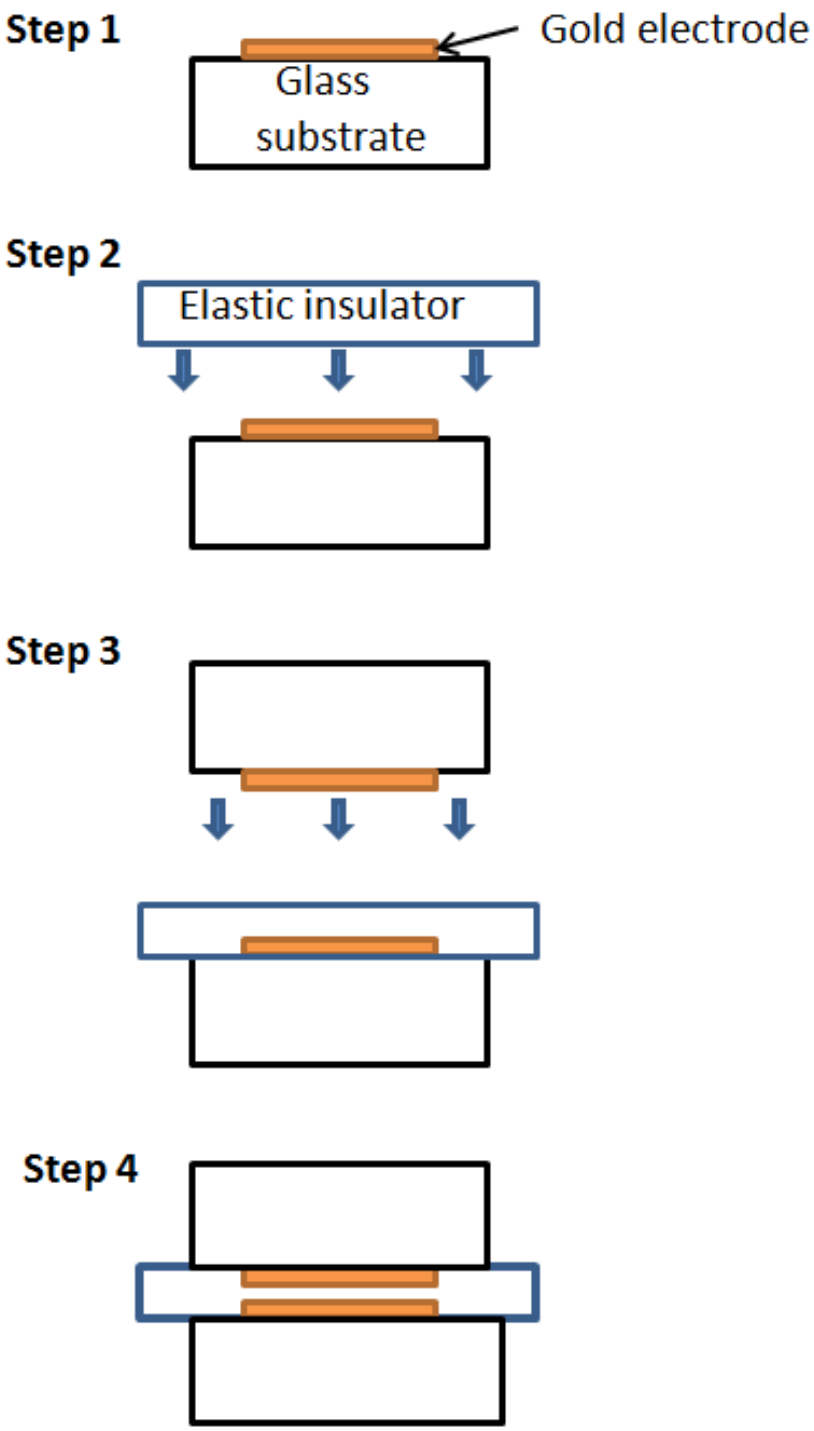

Figure. 3.2. Device fabrication process flow: Step 1 shows gold electrode deposited on glass disc; Step 2 shows bonding elastomer spacer to glass; Step 3 shows bonding the other glass having electrode to the other structure; Step 4 shows the final device structure (before coax cable connection).

Figure. 3.3. Photo of final structure of the device.

3.3. MEASUREMENT SETUP

To monitor the AC impedance levels during the course of device operation, the device was connected by shielded coaxial cables to an electrochemical potentiostat (Femtostat, Gamry). For the purpose of calibrating the biosensor device, a commercial load cell (LC302, Omega), capable of measuring load up to 500 lbs was used with its display meter (DP25BS-A, Omega) to read externally applied compressive load on the device.

A precision vise (EVSD-S60, Interstate) was used to manually apply external compressive pressure on the device to mimic the spinal loading mechanism after the implantation. The device and the commercial load cell were placed between the lower jaw and the upper jaw of the vise. The load cell was used to read the magnitude of the

load applied manually by lowering the upper jaw of the vise. The change in impedance value corresponding to pressure applied was converted to the load.

In order to determine the compressive modulus of the PDMS elastomeric insulator material, the precision vise along with the load cell and a digital microscope (KH-8700, Hirox) were used as shown in Figure. 3.4. Optical images were recorded to measure the change of PDMS thickness with the optical microscope to measure the strain developed in the PDMS material. Hence the values of applied compressive stress and corresponding value of strain on the elastomeric insulator enabled us to estimate its compressive modulus.

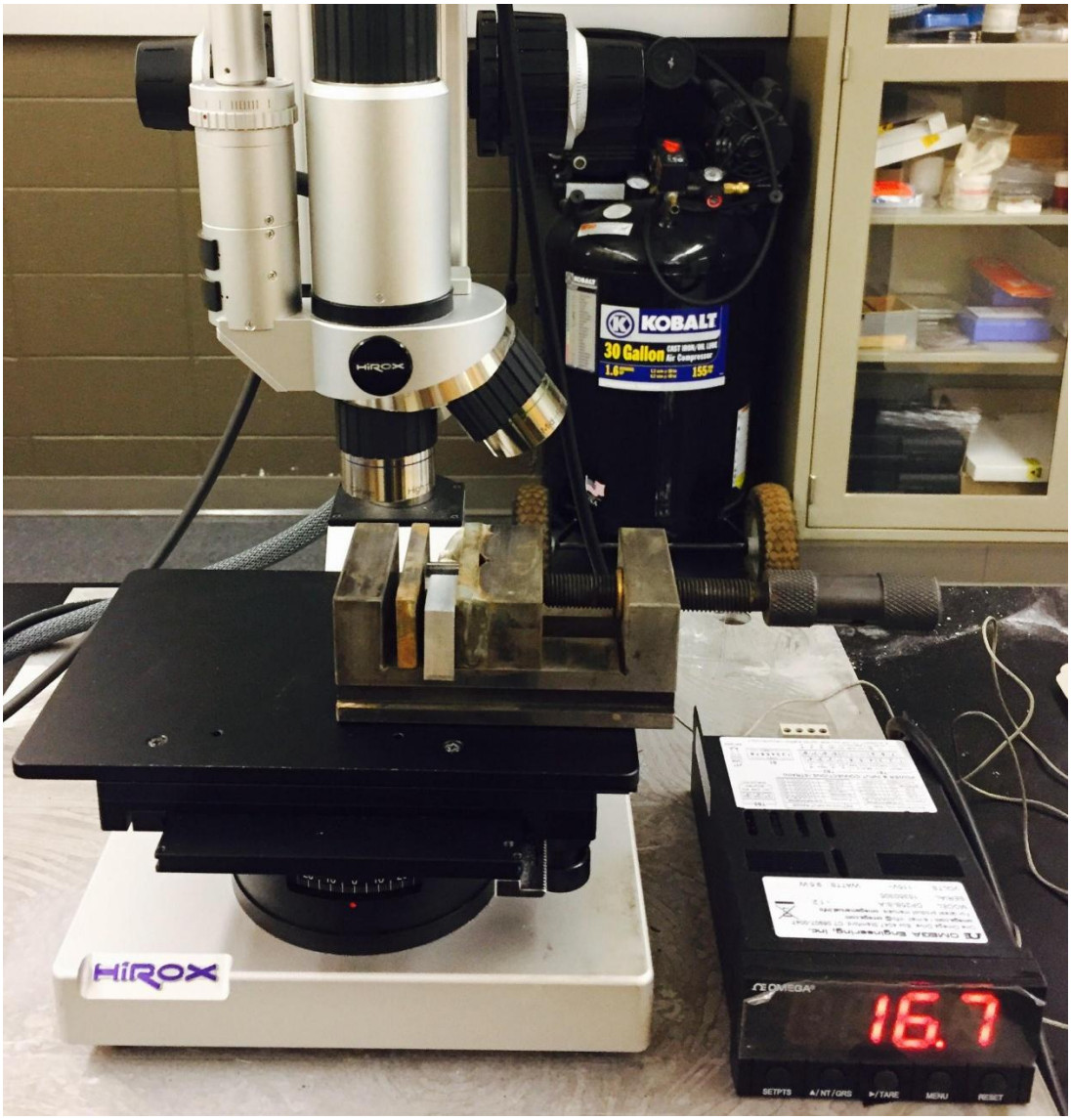

Figure. 3.4. Photo of compressive modulus measurement setup.

4. RESULTS AND DISCUSSIONS

4.1. SUBSTRATE DISSOLUTION

Glass substrate dissolution test was done in 2 L of phosphate buffer solution kept at 37 ^{o}C and stirred by a magnetic bar rotated at 60 rpm The dissolution test was performed in order to determine the weight loss rate, thickness reduction rate and diameter reduction rate of the disc-shaped glass substrates. The weight loss rate of the glass gives us an idea as to how long the substrate will take to totally dissolve inside the body. Particularly the thickness and diameter reduction rates of the glass substrates enable us to estimate the time duration for which the device can maintain its structural integrity or in other word its lifetime before it collapses and reaches 'sudden failure'.

Figure. 4.1. shows the linear weight loss rate of the glass substrates. It takes approximately 25 hours for each glass substrate weighing approximately 1 g to be totally dissolved in the solution. Since these samples do not have any slow-reaction layer, this time duration is not an indication regarding how long the device can remain functional (Figure. 2.3.stage A – stage B), rather it gives an estimate as to how long time the glass will take to get totally dissolved inside the body (Figure. 2.3.stage B – stage D).

Figure. 4.2. and Figure. 4.3. show the linear thickness reduction rate of each glass substrate and the diameter reduction rate, respectively. The thickness reduction rate is higher than the diameter reduction rate because of larger surface area of the top and bottom of glass substrate being exposed to solution than the sides. Figure. 4.4. shows photographic images of glass substrates during course of dissolution at 0 hour, 10 hour, 20 hour, 25 hour and 26 hour after immersion in solution, respectively. This rate can be

controlled by modifying the glass composition with higher percentage of silicate to achieve lower rates.

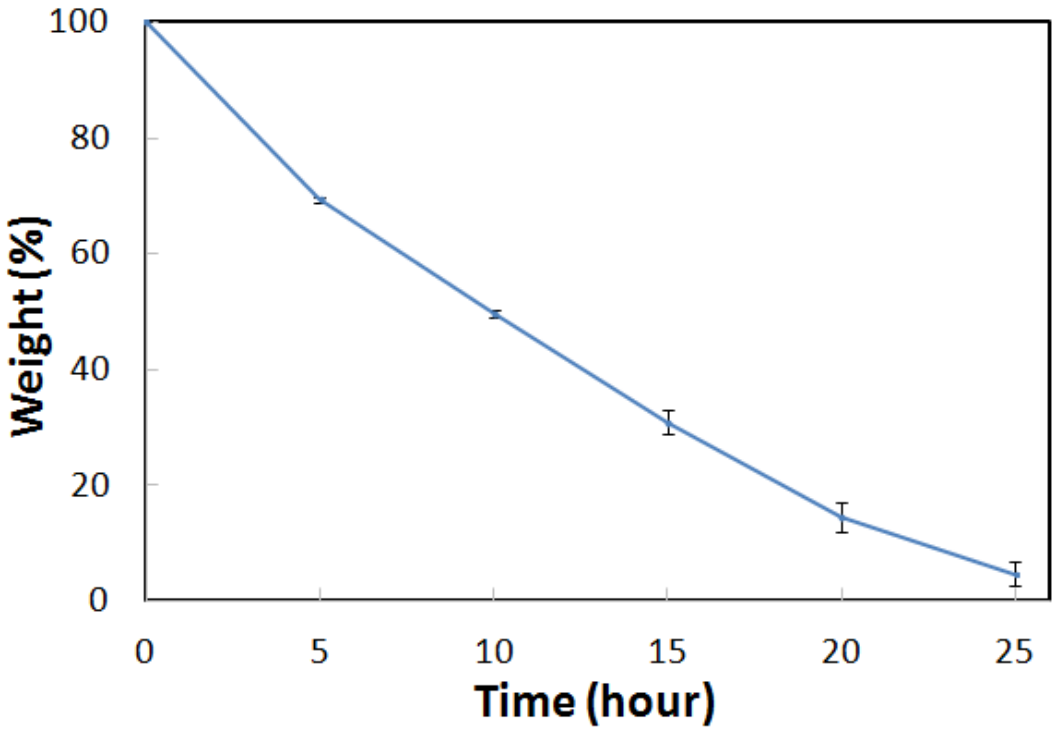

Figure. 4.1. Dissolution behavior of bare glass substrates (2.7 mm thick, 14 mm diameter, no coating/encapsulation) in phosphate buffer saline solution (pH 7.4 at 37^{o}C). (Weight % vs. time)

4.2. ELASTOMERIC INSULATOR THICKNESS

PDMS was used as the elastomeric insulator for the capacitive sensor. Important factors determining the mechanical property of PDMS include the base to agent mixing ratio, curing temperature and thickness. In our sensor design, having higher compressive modulus value of PDMS is preferred in order to accomplish the wider dynamic range of applied pressure. It was seen that the elastic modulus increases with increase in base-to-agent ratio up to 10:1 by weight, after which it decreases with higher ratio [16].

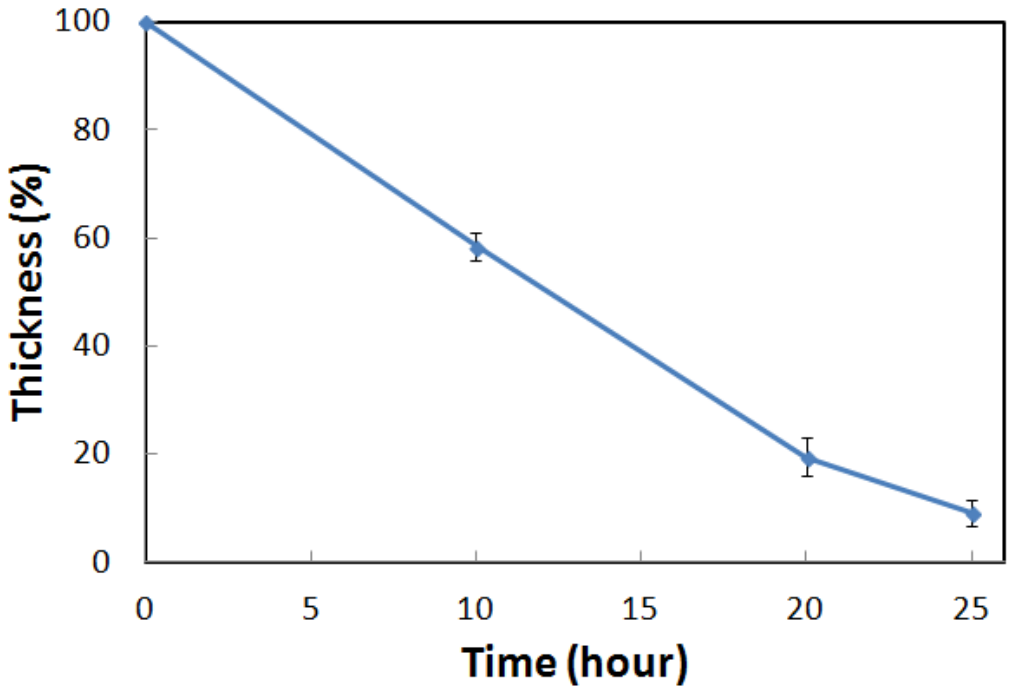

Figure. 4.2. Dissolution behavior of bare glass substrates (2.7 mm thick, 14 mm diameter, no coating/encapsulation) in phosphate buffer saline solution (pH 7.4 at 37^{o}C). (Thickness % vs. time)

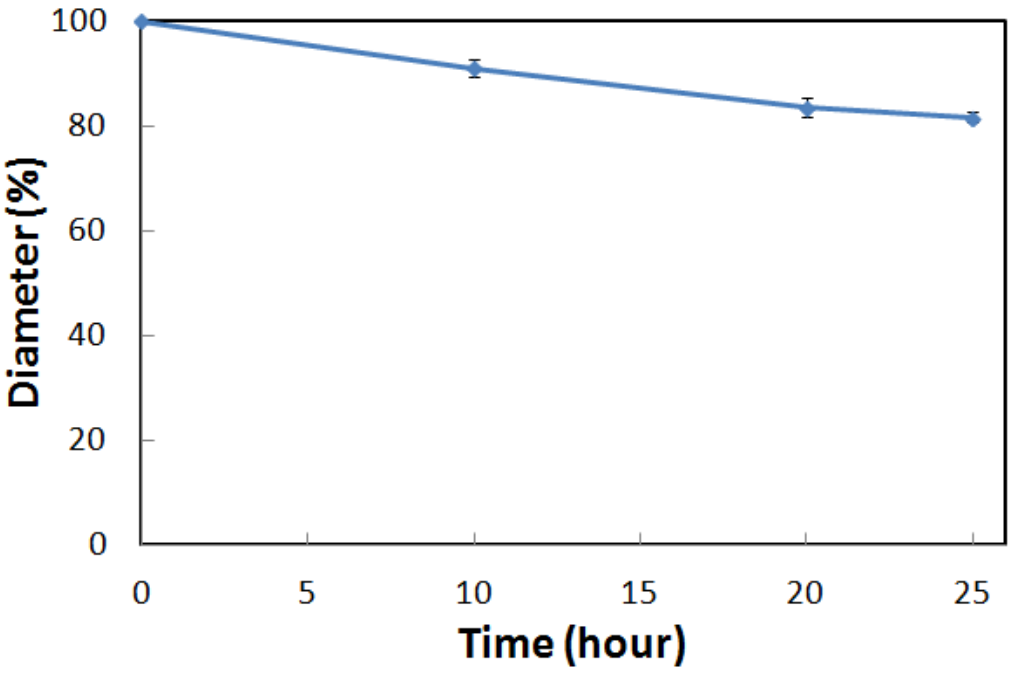

Figure. 4.3. Dissolution behavior of bare glass substrates (2.7mm thick, 14mm diameter, no coating/encapsulation) in phosphate buffer saline solution (pH 7.4 at 37^{o}C). (Diameter % vs. time)

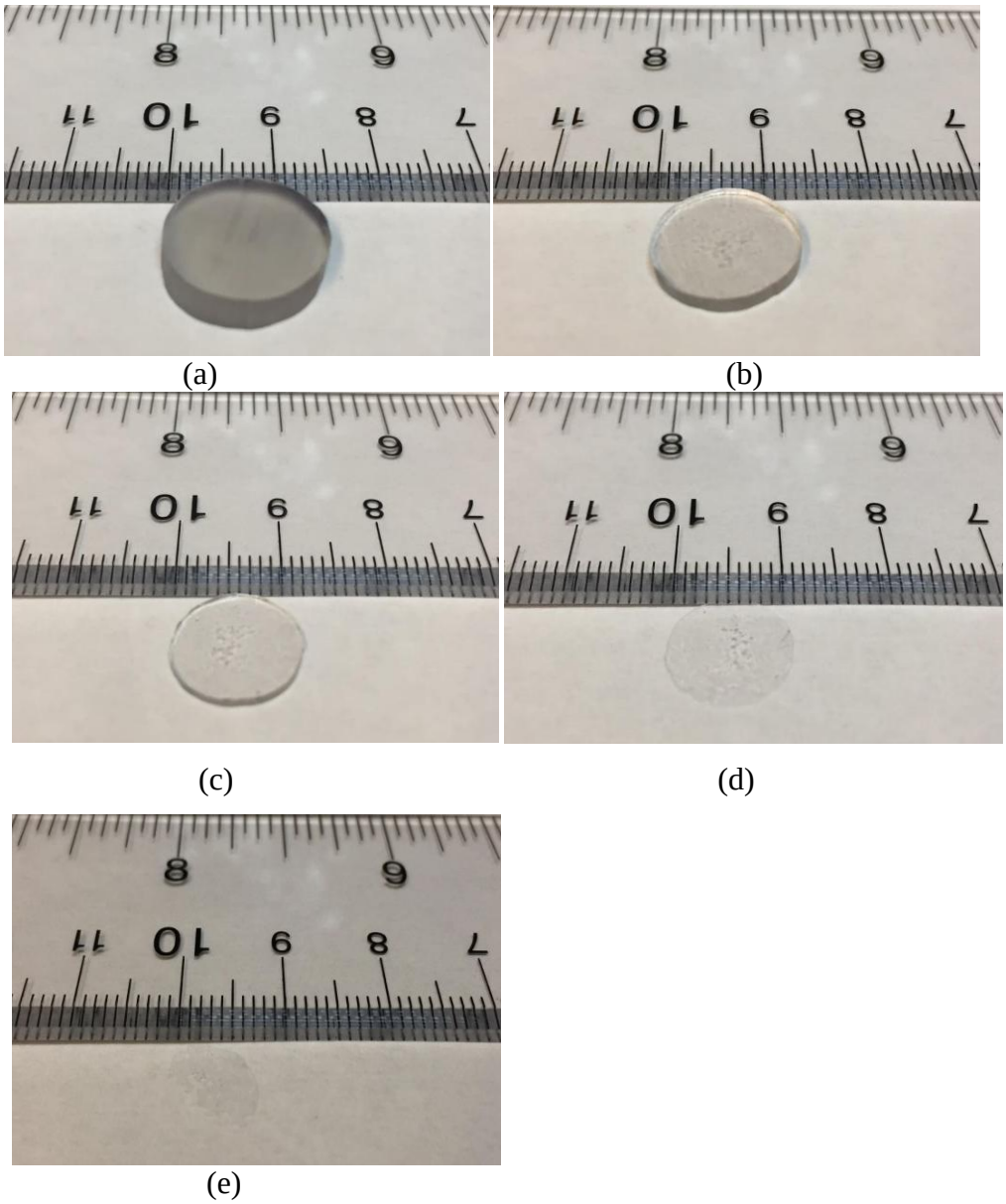

Figure. 4.4. Photographs of glass substrate taken at various stages of dissolution i.e. at (a) original, (b) 10 hours, (c) 20 hours, (d) 25 hours and (e) 26 hours in PBS (pH 7.4, 37 ^{o}C respectively.

Curing temperature of spin coated PDMS also had an effect on its compressive modulus as well. Curing at room temperature (i.e. 25 ^{o}C) for 48 hours produces the highest compressive modulus compared to higher curing temperatures as shown in Figure. 4.5 [17].

It was also reported that PDMS thickness above 200 µm exhibits bulk elastic property, in other words, PDMS samples as thin as 200 µm can retain their shape memory with repeated compressive force application [18]. The thickness of the PDMS after spin coating depends on the rpm, acceleration, spin duration, amount of PDMS poured and also surface property and area of substrate used. In this experiment, the rpm was varied to obtain the desired PDMS thickness of approximately 250 µm.

It was reported that the PDMS thickness is subject to fit to the experimental equation below:

$$W = 0.23\ \text{Ш}^{-1.14} \qquad (7)$$

where W is the thickness of PDMS in meter and Ш is the spin-coating speed in rpm [15]. Our desired thickness being 250 µm, using eq. (7), we get Ш = 450 rpm. This observation agrees well with our experimental data shown in Figure. 4.6., which indicates that the PDMS thickness of approximately 250 µm was obtained at 400 rpm for 30sec spin-coat time, base to agent mixing ratio of 10:1 by weight and curing temperature of 25 ^{o}C for 48 hours.

Traditionally silicon wafers are used as the substrate for spin-coating of many liquid phase materials. PDMS shows significant adhesion to the silicon wafer after curing and hence peeling off the PDMS sheets from the wafers becomes difficult. Often this results in rupturing of sheets during peel off unless a sacrificial layer is applied on the silicon wafer prior to PDMS spin-coating. In our experiment, ethanol-cleaned and air-dried, acrylic sheets (Optix, 2 mm thick, Plaskolite Inc.) were used as the substrate for spin-coating PDMS.

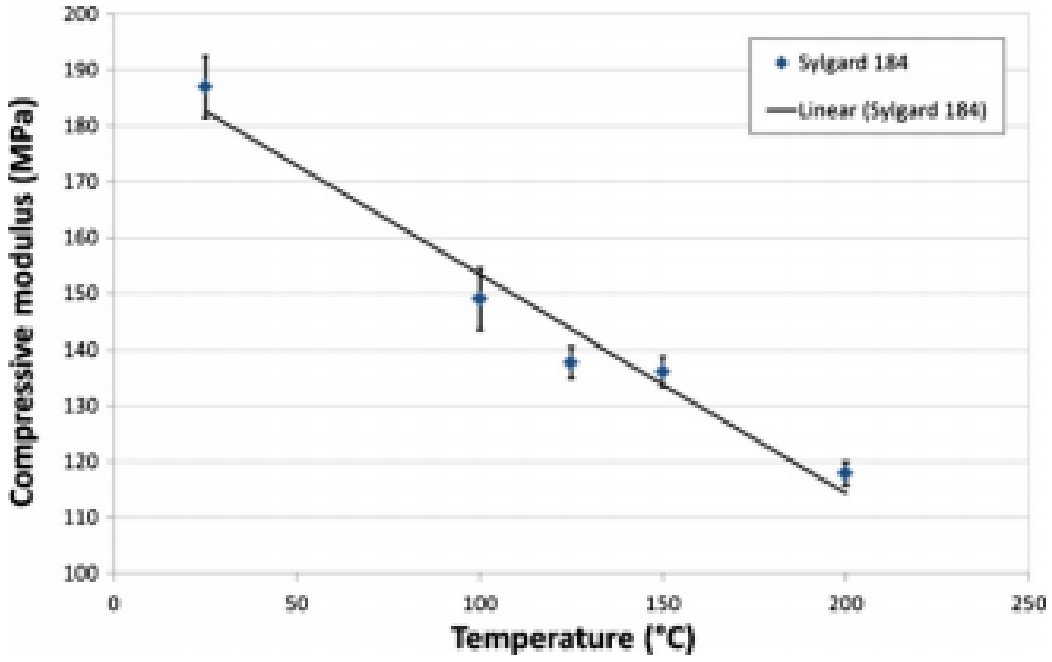

Figure. 4.5. Compressive modulus of PDMS elastomer vs. curing temperature for sample preparation according to ASTM D575-91 standards [after 17].

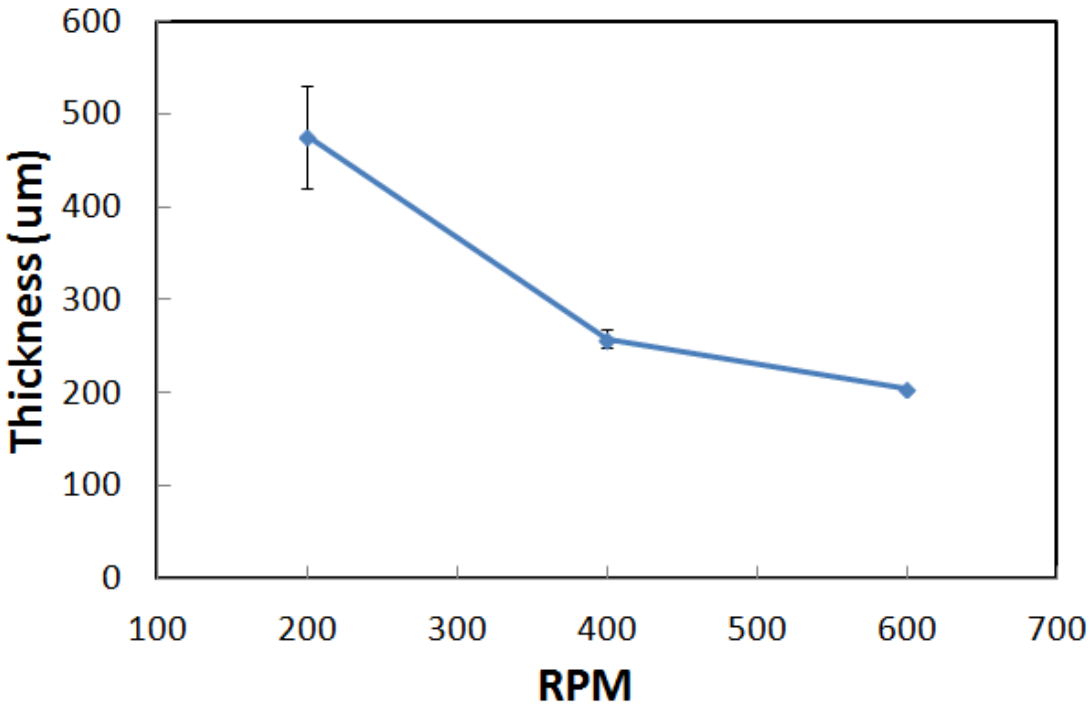

Figure. 4.6. Variation of thickness of PDMS elastomer vs. spin speed for preparation.

Although quantitative analysis of adhesion between acrylic sheet and PDMS was not conducted by peel test, it was observed that cured PDMS sheets was easily peeled off from the acrylic substrate without the need of using any additional sacrificial layer. Hence, acrylic sheet is an excellent substitute as substrate for spin-coating PDMS due to its low adhesion property to PDMS.

4.3. COMPRESSIVE MODULUS OF ELASTIC INSULATOR

Mechanical characterization was conducted to determine the compressive modulus (CM) of the PDMS elastomer. The compressive stress-strain plot enables us to determine the dynamic range of the pressure sensor that is the linear region of the plot. This means the sensor has repeatability in that linear range, based on the elastomer's shape-retention capability within that pressure range.

The CM plot of the elastomer was obtained by applying known compressive force to the elastomer sample manually using the precision vise and load cell to measure the corresponding deformation. Figure. 4.7. shows photographic images of PDMS thickness taken by Hirox microscope at: no load applied (0 MPa) and then upon compression by with increasing load up to 14.35 MPa and finally after removal of the load. The strain developed at each stress value were graphically measured to generate the CM plot shown in Figure. 4.8. The CM was approximately 119 MPa which is in the same order obtained for PDMS samples prepared in accordance with American Society of International Association for Testing of Materials (ASTM) D575-91 standards. For this case, test specimens were approximately 28 mm in diameter and 12.5 mm thick and tested using ASTM D1229-03 (2008) methods to obtain a CM of approximately 187 MPa [17].

Although according to ASTM D575-91 (Reapproved 2012), comparable CM results are obtained only when the tests are made on samples of exactly same dimensions tested to the same percentage of deflection or tested under the same force, our sample's CM value is in similar range to the one obtained by ASTM procedure.

4.4. FREQUENCY RESPONSE

Eqs. (5) and (6) indicate that impedance of a capacitor is inversely related to the operating frequency. Figure. 4.9. shows the typical frequency responses of three capacitive devices. A frequency sweep from 1 KHz to 100 KHz at 500 mV rms was given and the corresponding impedance values were measured and plotted by the impedance meter. These plots are in agreement to the mathematical equations enables us to select a particular frequency to operate the device. Based on the geometry of capacitive device (thickness 250 μm, area 50.26 μm^2, ε 2.7), the calculated value of 7.5 pF is in similar range of 7.14 pF when measured.

In actuality, it is preferable to work with low power applications for implantable medical devices. Since supply voltage is fixed, in order to minimize the capacitor current, the operating frequency should be low and this could be understood from the eq. 8:

$$I_C = C\, dV/dt \qquad (8)$$

where I_C is the capacitor current and dV/dt is the rate of change of voltage with time and is directly proportional to the operating frequency.

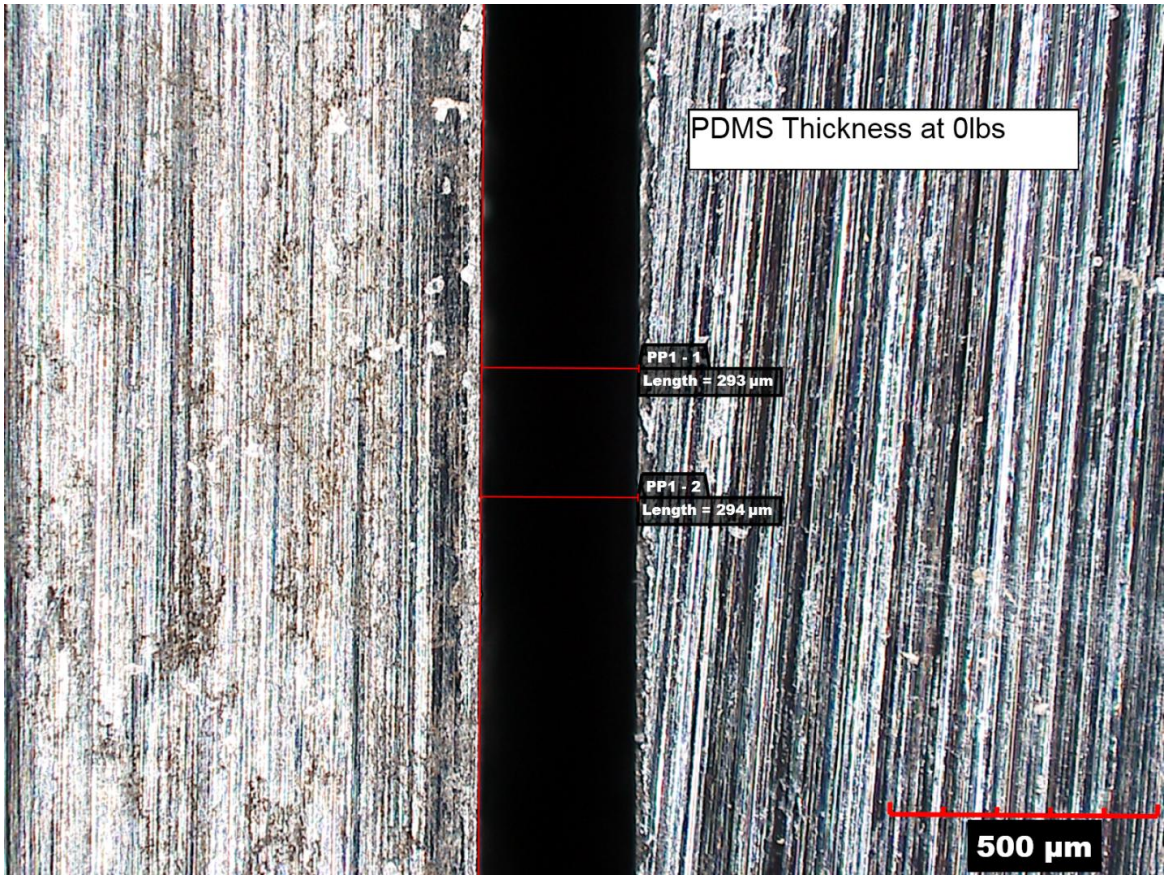

(a)

Figure. 4.7. Optical microscope images of PDMS elastomer (a) taken during compression at 0 lb, (b) taken during compression at 40 lbs, (c) taken during release of 40

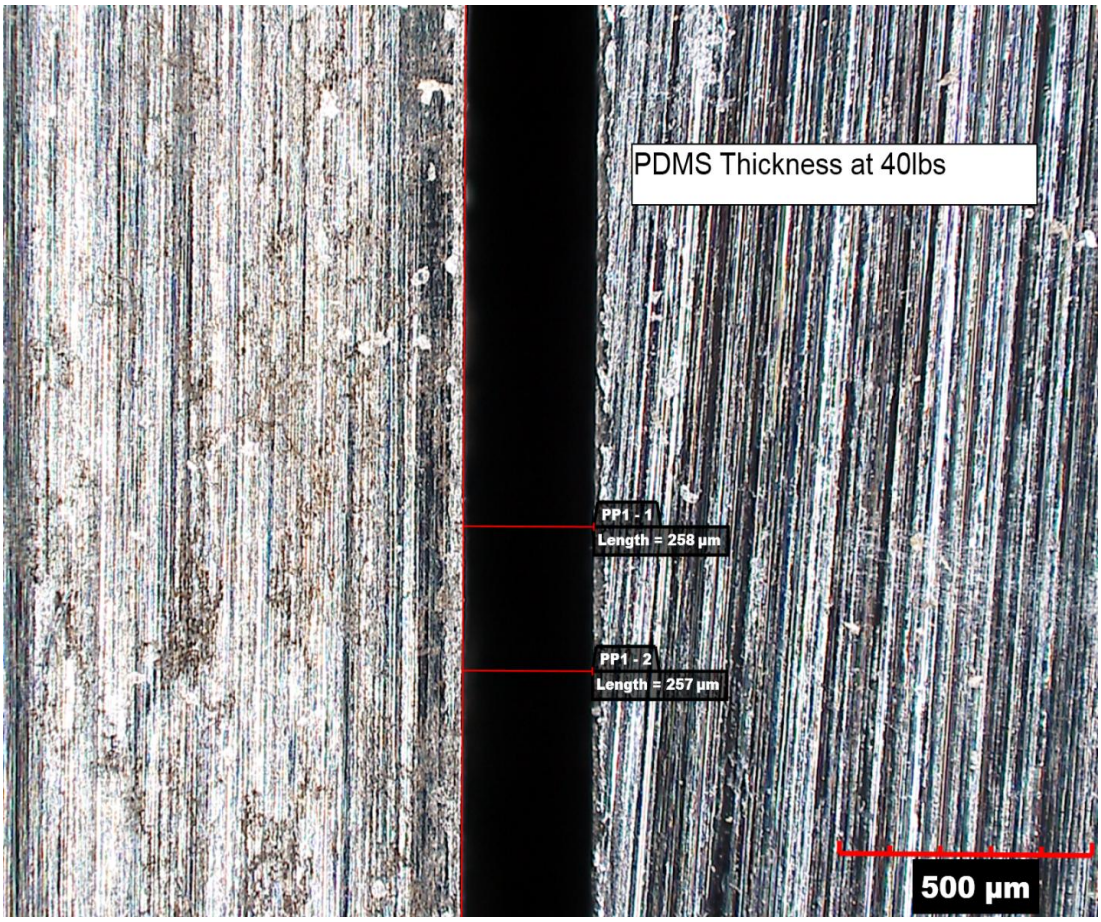

(b)

Figure. 4.7. Optical microscope images of PDMS elastomer (a) taken during compression at 0 lb, (b) taken during compression at 40 lbs, (c) taken during release of 40 (cont.).

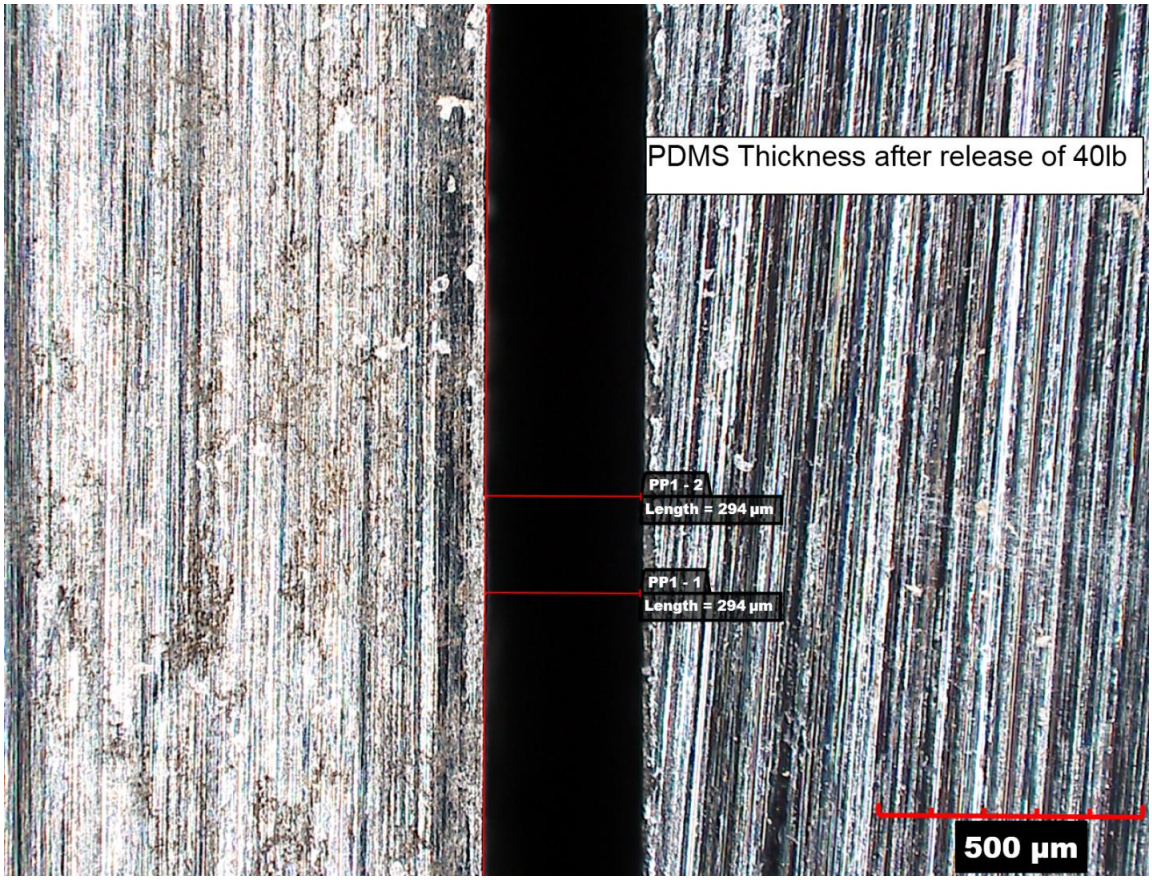

(c)

Figure. 4.7. Optical microscope images of PDMS elastomer (a) taken during compression at 0 lb, (b) taken during compression at 40 lbs, (c) taken during release of 40 (cont.).

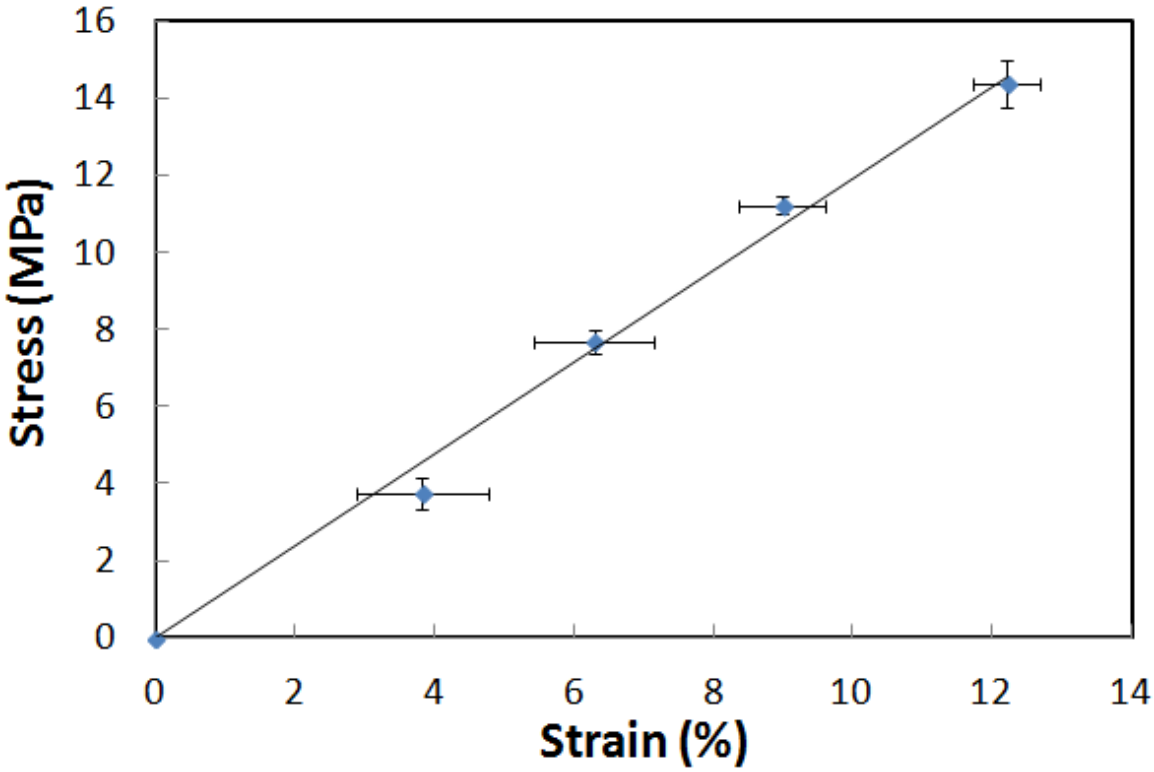

Figure. 4.8. Compressive modulus of PDMS elastomer (thickness approximately 250 µm) used as pressure-sensitive element.

Hence keeping these factors in mind, all the sensor data obtained in this experiment was conducted at an operating frequency of 1 KHz although higher frequencies till 100 KHz are expected to work well too. It was also seen that operating sinusoidal voltage around 100 mV rms generated approximately 3.48 % output signal fluctuation due to system noise compared to 500 mV which generated fluctuation approximately 0.3 %. Hence 500 mV was chosen as the operating voltage. Although in latter application higher rms voltages can be used as it will be beneficial in increasing signal-to-noise ratio.

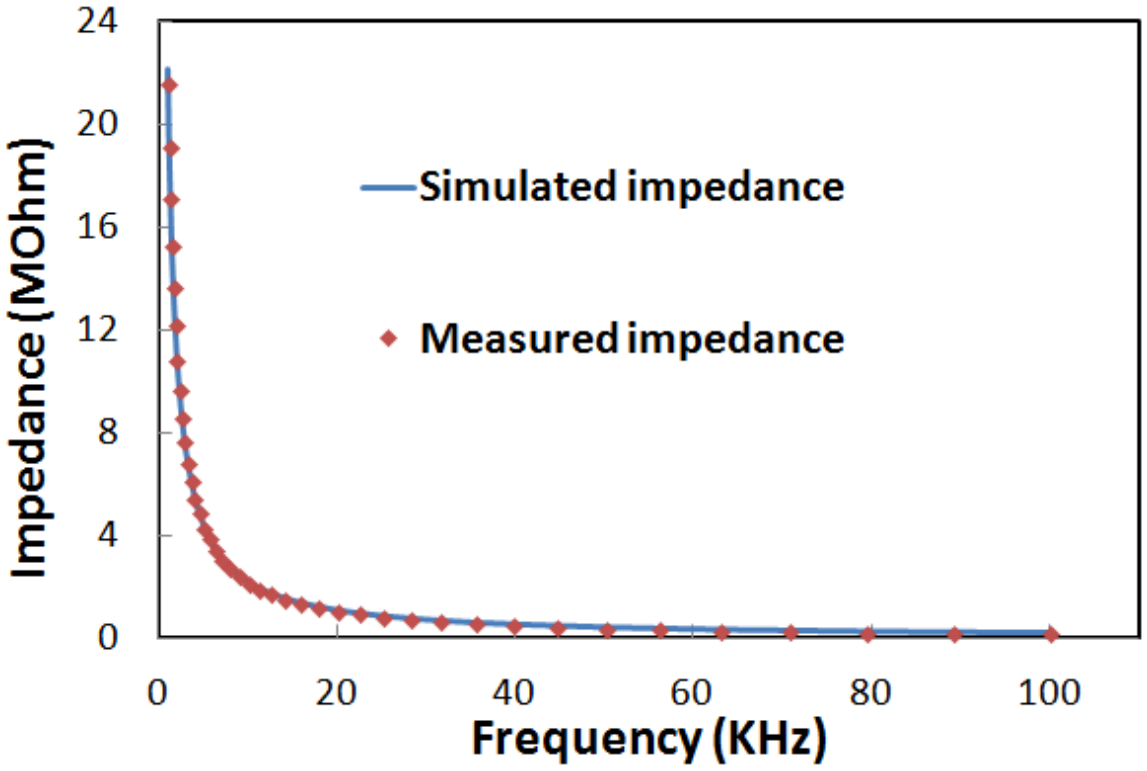

Figure. 4.9. Frequency vs. normalized impedance (at 500 mV rms)

4.5. PRESSURE SENSITIVITY

Time response plots are indicative of device's ability to respond to pressure application with respect to time. Time responses were obtained by repeated application of various known pressures between 3.59 MPa to 14.35 MPa (equivalent to 5 lb to 40 lb) manually applied with the precision vise. The measurements were carried out at 500 mV rms voltage and 1 KHz operating frequency. Figure. 4.10. (a),(b),(c) shows the time response of three devices. The lower impedance value regions indicate pressure is applied during that time interval leading to proportional decrease in impedance. The consequent recovery of impedance upon removal of pressure the original baseline reversibly indicates excellent shape memory retention of the elastomeric PDMS insulator serving as

the pressure-sensitive element. The values of impedance for specific pressures are well in agreement to the CM plot of PDMS.

Figure. 4.11. shows the pressure sensitivity curve of devices where the percentage increase in capacitance was plotted for an increment of approximately 1.8 MPa (corresponds to 5 lbs) over a range of 0 MPa to 14.35 MPa (corresponds to 40 lbs). The percentage increase in capacitance for its corresponding pressure is well in accordance to the CM plot obtained for PDMS, thereby re-validating the device successful operation.

4.6. DISSOLUTION BEHAVIOR

The dissolution behavior of the device is the proof-of-concept of the stage B to C in Figure. 2.3. followed by rapid disintegration. The time response was monitored during device dissolution. Figure. 4.12. (a) shows that the device impedance maintains at a constant level followed by steep decrease after approximately three hours. This change clearly demonstrated the expected behavior of rapid failure. During dissolution, the solution consumes outer portion of the device thereby dismantling the structure. As a result, the two electrodes become short-circuited through the conductive solution and the impedance of the device is drastically reduced.

Figure. 4.12. (b) and (c) shows the device performance inside solution when pressures were repeatedly applied at some regular time intervals. The low impedance region shows that pressure was applied for some time duration. The higher impedance region indicates that pressure was removed resulting in shape memory retention of the elastomeric PDMS in the capacitive device and hence resetting the device. After a few

hours of periodic pressure application, the device impedance steeply decreased indicating the collapse of entire structure. This proves that the device worked successfully under pressure application during the stage B to C followed by structural disintegration and consequent sudden failure.

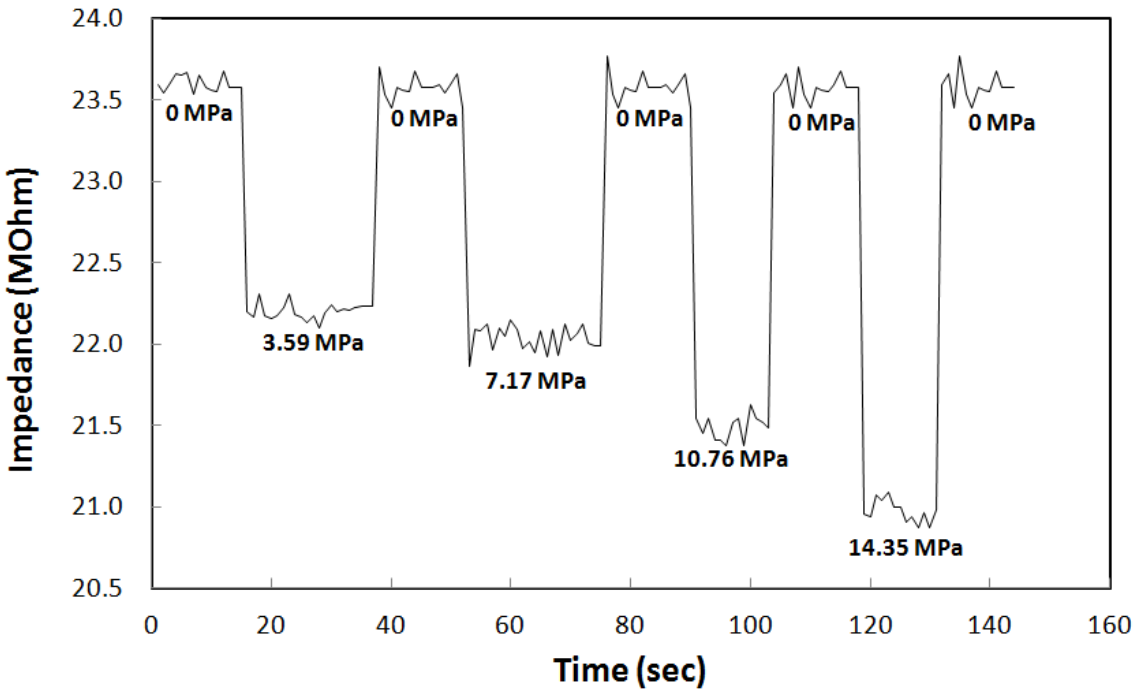

(a)

Figure. 4.10. Typical time response plots of three devices carried out with operating sinusoidal voltage (500 mV rms, 1 KHz)). (a)Device 1, (b) Device 2, (c) Device 3.

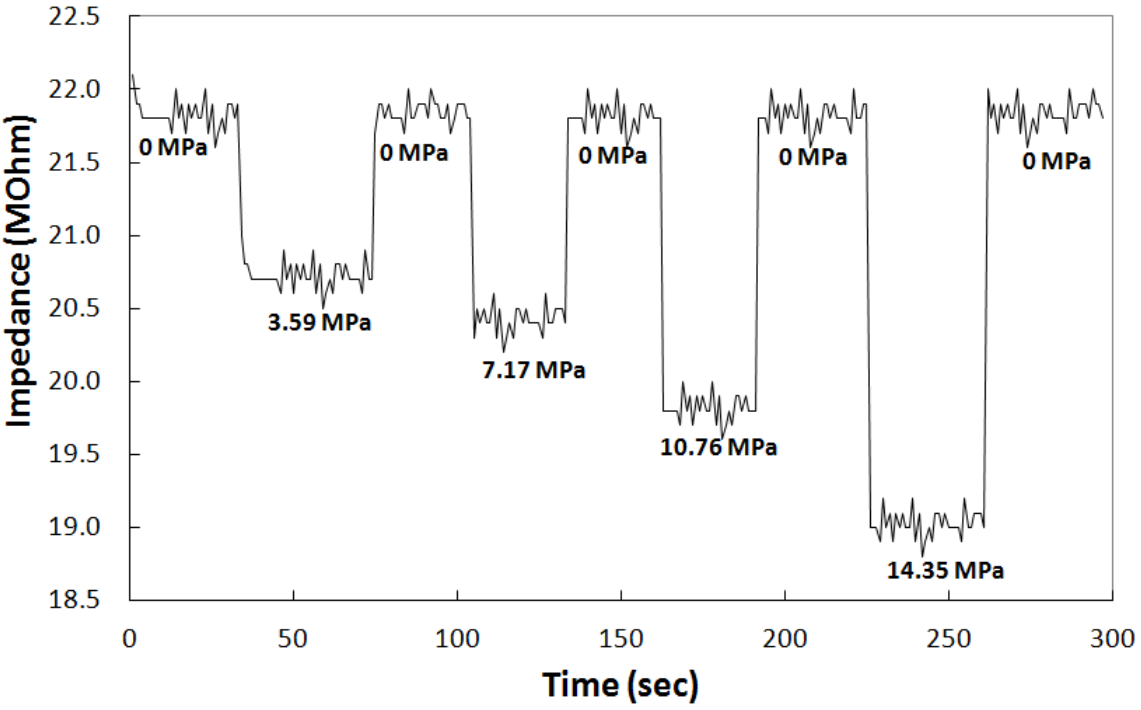

(b)

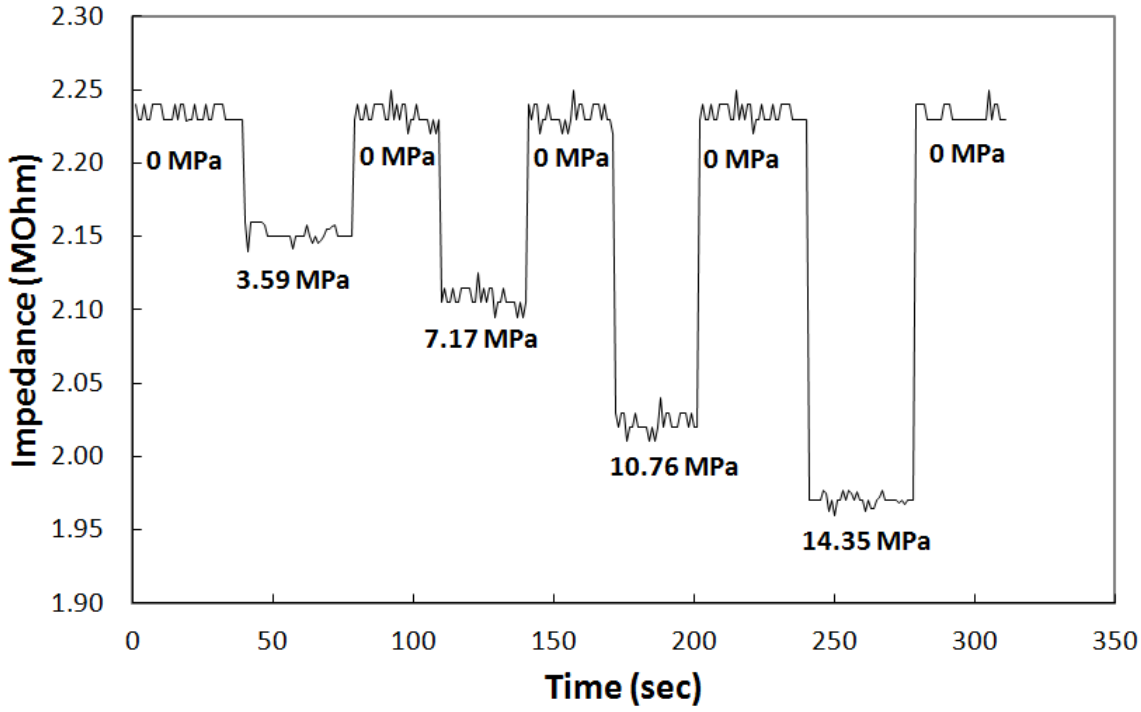

(c)

Figure. 4.10. Typical time response plots of three devices carried out with operating sinusoidal voltage (500 mV rms, 1 KHz)). (a)Device 1, (b) Device 2, (c) Device 3.(cont.).

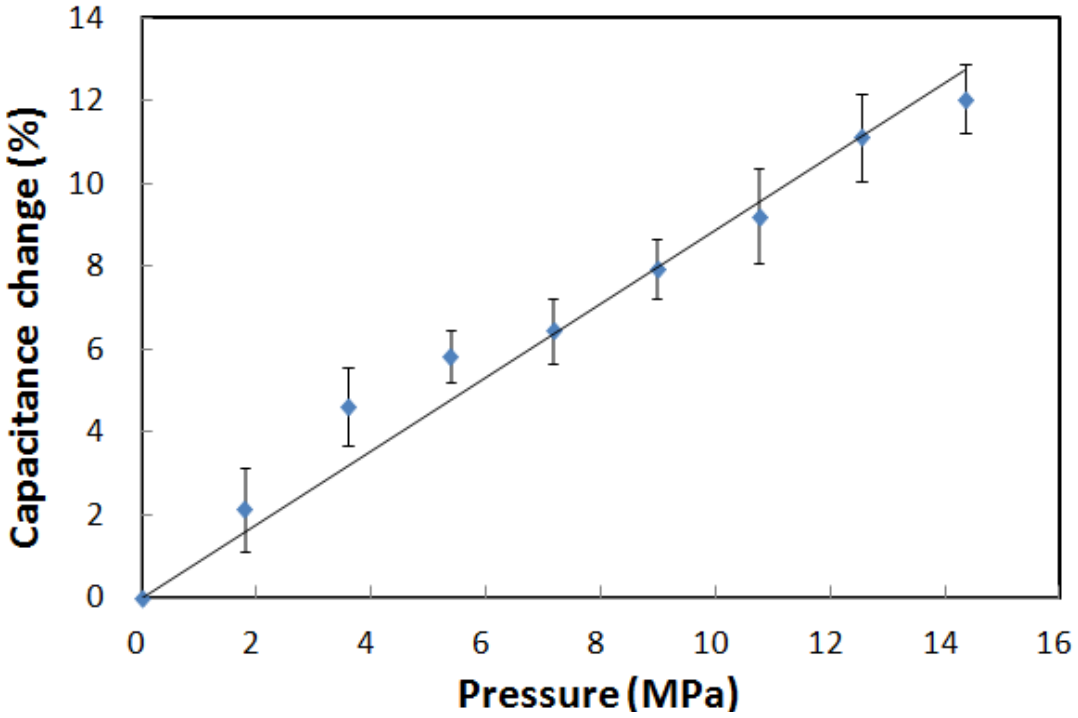

Figure. 4.11. Pressure sensitivity of five devices taken at 500 mV and 1 KHz operating frequency (n=5)

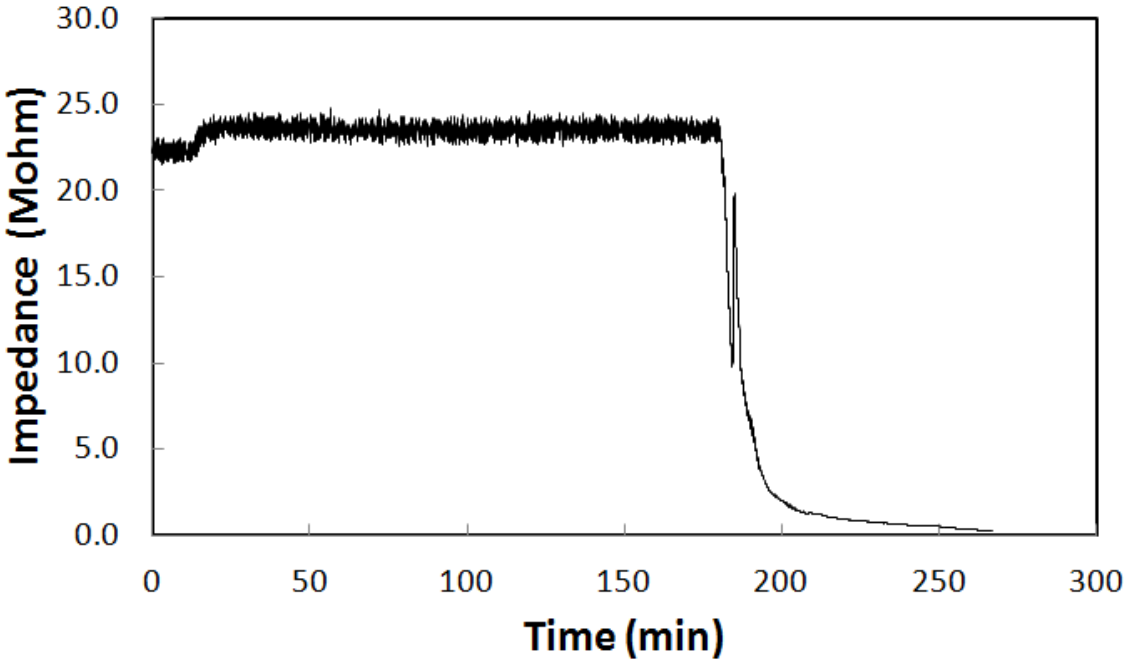

Figure. 4.12. (a) Dissolution behavior of device in phosphate buffer solution (ph 7.4, 37 ^{o}C) to demonstrate the sudden failure (stage B to C in Figure. 2.3) with no applied pressure.

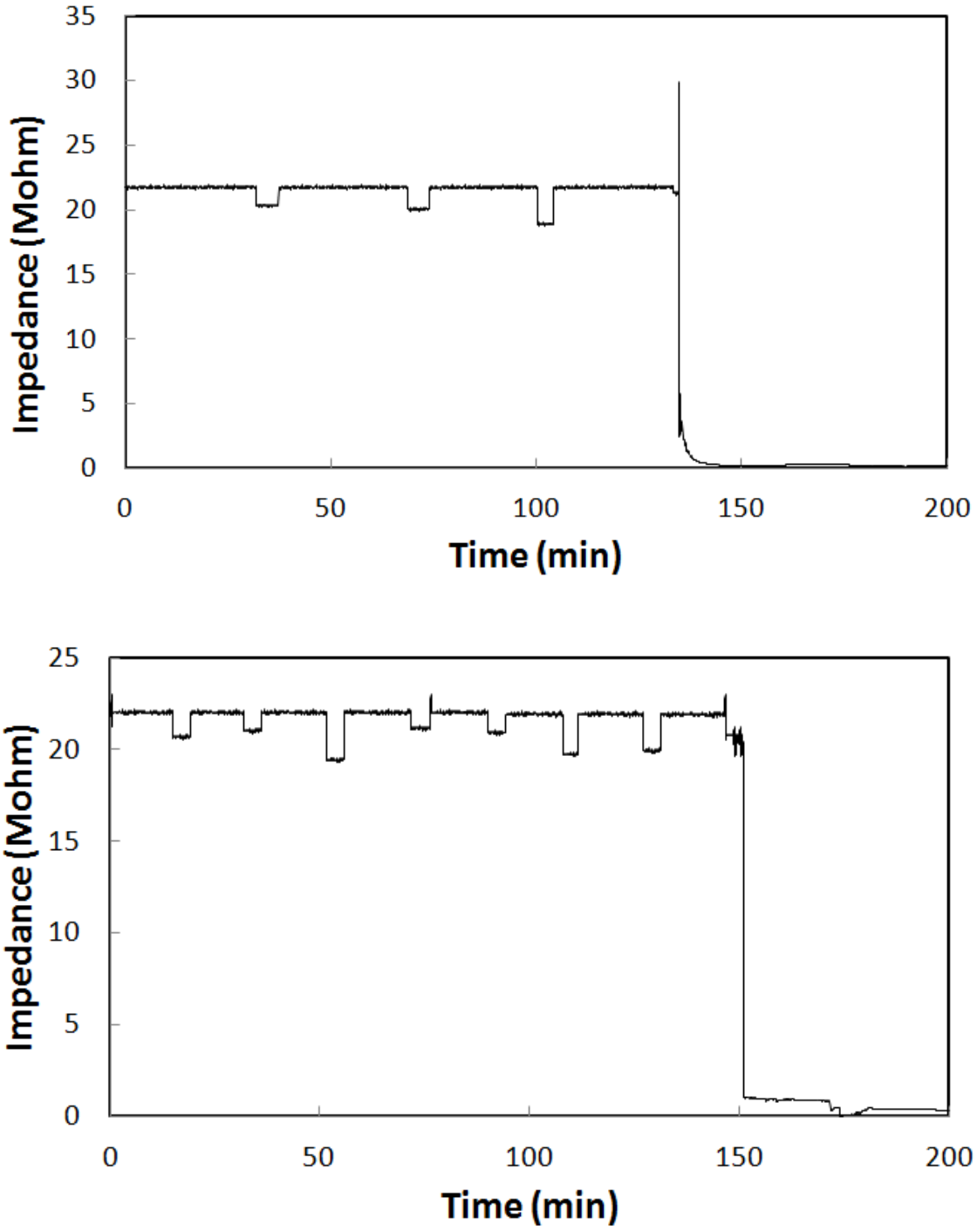

Figure. 4.13. Dissolution behavior of device in phosphate buffer solution (ph 7.4, 37 ^{o}C) to demonstrate the sudden failure (stage B to C in Figure. 2.3) with repeated sporadic applied pressure.

5. CONCLUSION

Borate-based biodegradable glass material is successfully used as a novel functional platform to fabricate solid state sensors towards temporary implantation. The capacitive sensor responded to compressive pressure within range of approximately 14 MPa with good repeatability. The device remained operational for a short intended lifetime before it was disintegrated and finally dissolved, thereby validating the proof-of-concept of biodegradable sensors. Hence by optimizing design and fabrication parameters, it is expected to realize fully functional biodegradable devices during operational lifetime followed by rapid disintegration.

Therefore, the use of biodegradable glass substrates is expected to be a viable approach to develop reliable temporary implants for interventional and monitoring purposes. This is anticipated to create a whole new class of implantable biomedical device that can revolutionize the present healthcare system.

APPENDIX A.

PROCEDURE FOR PREPARING BORATE GLASS WAFERS

Bioactive borate glass wafer is prepared by first making glass rods and by then slicing it into wafers using a low speed saw (Isomet, Buehler). Preparation procedure for glass rods and wafers is described in Table A.1. Glass composition is given in Table A.2.

The glass wafers were then mounted on an aluminum holder using a thermo plastic product, Brewerbond 220 (Brewer Science, Rolla, MO), so that they can be clamped into a specimen holder and then polished using an automatic polisher (Tegramin30, Struers). Mounting procedure is described in Table A.3. Table A.4 and A.4.5 covers the detailed procedure polishing and grinding.

After the polishing the wafers were then demounted and cleaned. Table A.6 records the procedure for demounting and cleaning glass wafers.

Table A.1. Preparation Procedure for borate glass rods and wafers

Sr. No.	Procedure
1	- Melting sodium tetraborate ($Na_2B_4O_7$) in a platinum crucible for 30 minutes at 1000˚C - Stirred every fifteen minutes using a pure silica rod
2	- Poured into stainless steel cylindrical molds preheated to 200˚C - annealed at 450˚C for 30 minutes - Cooled slowly (furnace normal cooling rate) to room temperature
3	- Cylindrical glass rod of approximately 1.4 cm diameter and 3cm length was formed - Glass rod formed is then wrapped using an insulation tape and mounted on the saw - A small weight is applied on the saw arm and the instrument was setup at 6 rpm - Glass wafers formed were 3~4 mm and afterward cleaned using acetone

Table A.2. Material composition for borate glass rods and wafers

Component	Wt %	Mol %
B_2O_3	69.2	66.7
Na_2O	30.8	33.3

Table A.3. Mounting procedure for wafers

Sr. No.	Procedure
1	- Aluminum holder cleaned with acetone - Top surface of holder coated with a thin layer of Brewer Bond 220
2	- Holder heated on a hot plate - At 80^{o} C for 5 minutes - At 130^{o} C for 5 minutes - At 180^{o} C for 5 minute - Cooled to room temperature
3	- Holder again heated to 130^{o} C - Glass wafer was placed on top and slightly pressed - Cooled to room temperature - Very strong bonding between the glass wafer and the aluminum holder

Table A.4. Procedure for polishing and grinding glass wafer

Sr. No.	Procedure
1	- Six aluminum holders mounted with glass wafers were clamped in a specimen holder - Insert the holder in the automatic polisher(Tegramin30, Struers)
2	- Mount MD-Gekko (300 mm magnetic pad for attaching SiC foils) on MD-Disc (drive plate) - An alcohol based lubricant (DP-Lubricant Yellow, Struers) is used just enough to keep the surface moist through all the polishing and grinding steps
3	- Drive plate is set at 300 RPM* - Head is set at 150 RPM - Co-rotation of both drive plate and head (drive plate 300 RPM, head 150 RPM)

* Drive plate is set at 150 RPM for diamond polishing stage

** Same rotation speed for drive plate and head might result in better polishing as it may damage the surface of the wafer less

Table A.5. Sequential polishing and grinding with different grit size

Step No	Grit Size (um)	Polishing Agent	Force (N)	Time/Removal
1	76	SiC foil	90	30 seconds
2	32.5~36	SiC foil	90	100 um
3	16.7~19.7	SiC foil	90	50 um
4	4.5~6.5	SiC foil	90	1 minute
5	3	Diamond Suspension	60	3 minutes
6	1	Diamond Suspension	60	3 minutes
7	0.25	Diamond Suspension	60	3 minutes

Table A.6. Procedure for demounting and cleaning glass wafer

Sr. No.	Procedure
1	- Aluminum holders heated to a temperature of 130^{o} C - Wafers were slid off the holders
2	- Wafers were cleaned ultrasonically in 1-Dodecene twice for 15 Minutes each - Ultrasonication was done in isopropanol for 15 minutes - Wafers were wiped clean using 100% continuous polyester wipes (TX 1009 Alpha Wipe) - Wafers were sprayed with isopropanol and then blown dried using high purity nitrogen gas.

APPENDIX B.

PROCEDURE FOR METAL ELECTRODE PATTERNING

Borate glass wafers were patterned with gold film using a shadow mask.

Table B.1. Methods used for deposition of gold

Method	Working parameters
Shadow mask	- OHP sheet - Diameter of 8mm was cut out using punching machine; 2mm wide and 3mm long trace line was cut out using scissors.
Gold deposition (Biorad E5400)	- Gas: Argon - Working Pressure: 80 millitorr (Argon) - DC Current: 20 mA - Deposition time: 3 minutes

APPENDIX C.

PROCEDURE FOR MECHANICAL CHARACTERIZATION OF PDMS

PDMS sheet was fabricated at 400 RPM and cured at room temperature. Now square shaped PDMS pieces of area equivalent to the sensor area are cut out and placed on the lower jaw of the precision vise. Then another rigid metal bar was placed just touching the side of the PDMS piece followed by placement of the commercial load cell and upper jaw of the vice.

This entire setup was placed horizontally under Hirox Digital Microscope. The upper jaw was now manually pushed towards the sensor giving a compression force. The shrinkage /reduction in PDMS thickness corresponding to the known applied pressure displayed by the commercial load cell meter were observed. Compression force of 10lb, 20lb, 30lb, 40lb was applied each for 1 minute and then removed. It was observed that the PDMS goes back to its original thickness upon removal of pressure, hence validating its shape memory property.

The obtained strain value and pressure value gave the compressive modulus of the PDMS fabricated sensor.

Figure. C (a),(b),(c),(d),(e),(f) shows the compression test images taken by Hirox Digital Microscope.

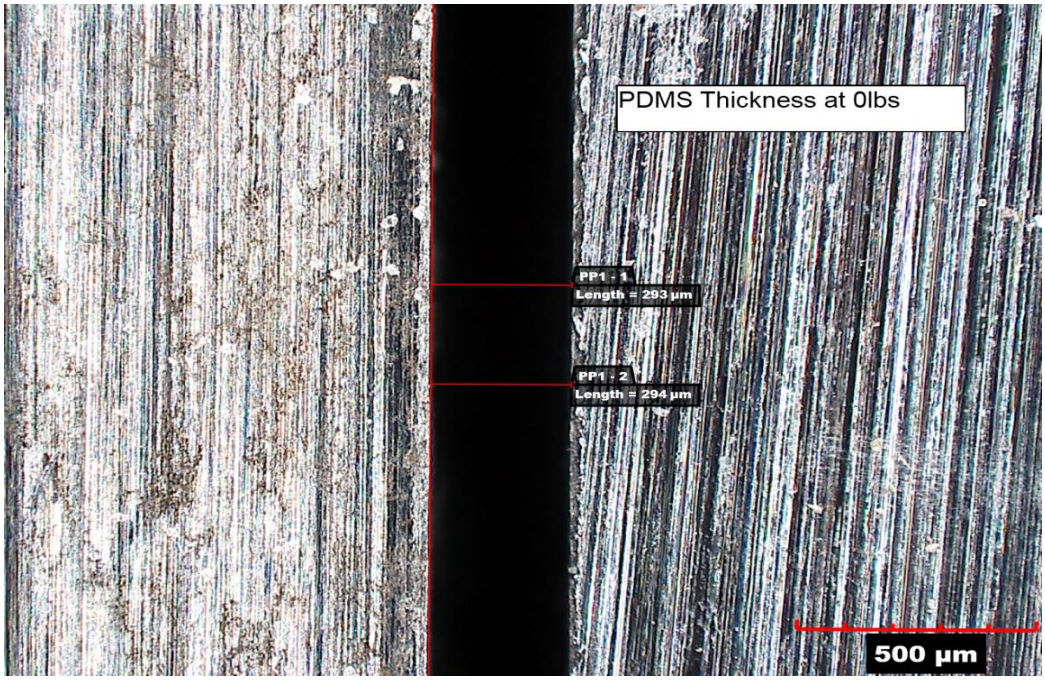

Figure C. Compressed thickness at various applied load (a) 0 lbs.

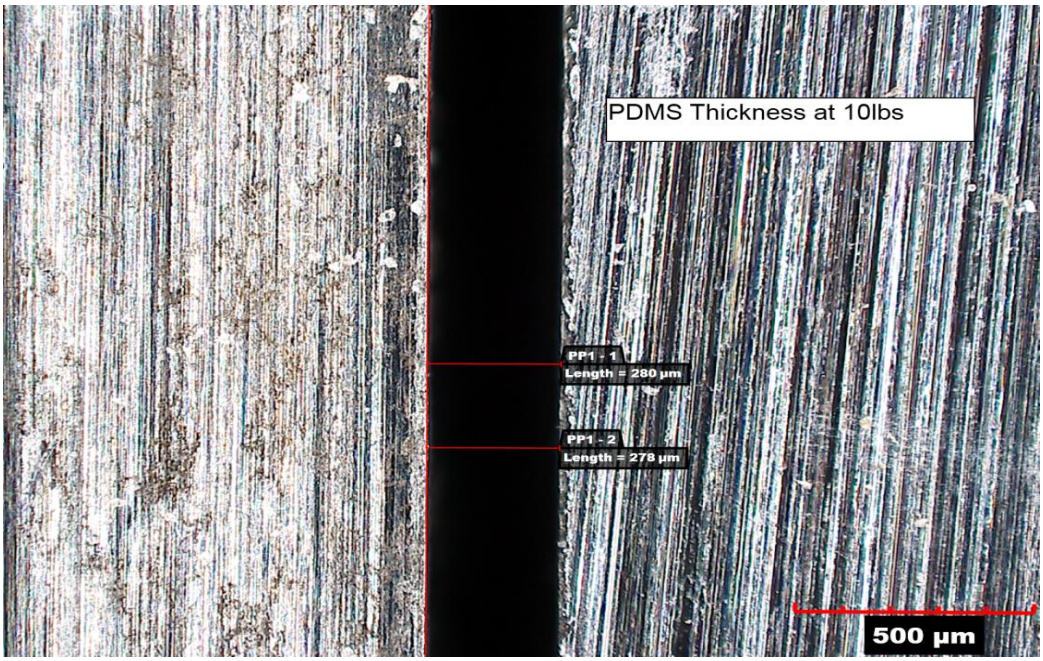

Figure C. Compressed thickness at various applied load (b) 10 lbs (cont.).

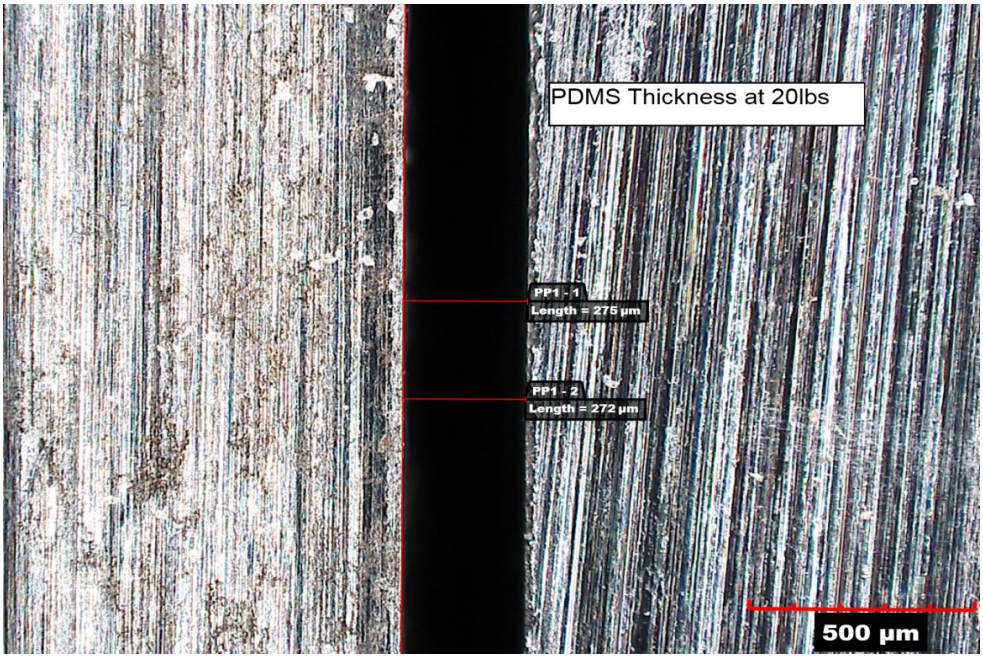

Figure C. Compressed thickness at various applied load (c) 20 lbs (cont.).

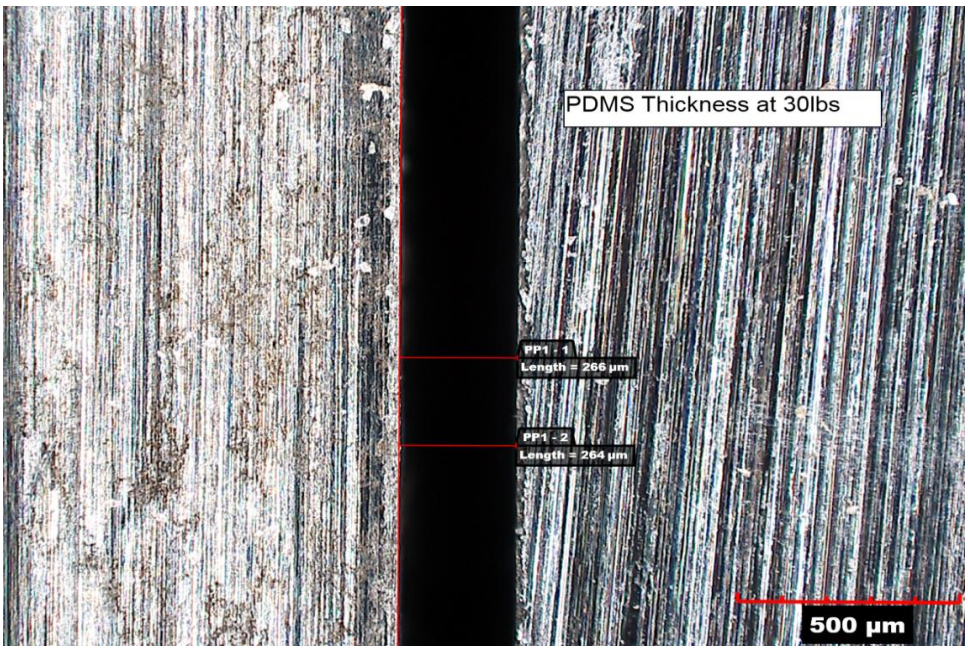

Figure C. Compressed thickness at various applied load (d) 30 lbs (cont.).

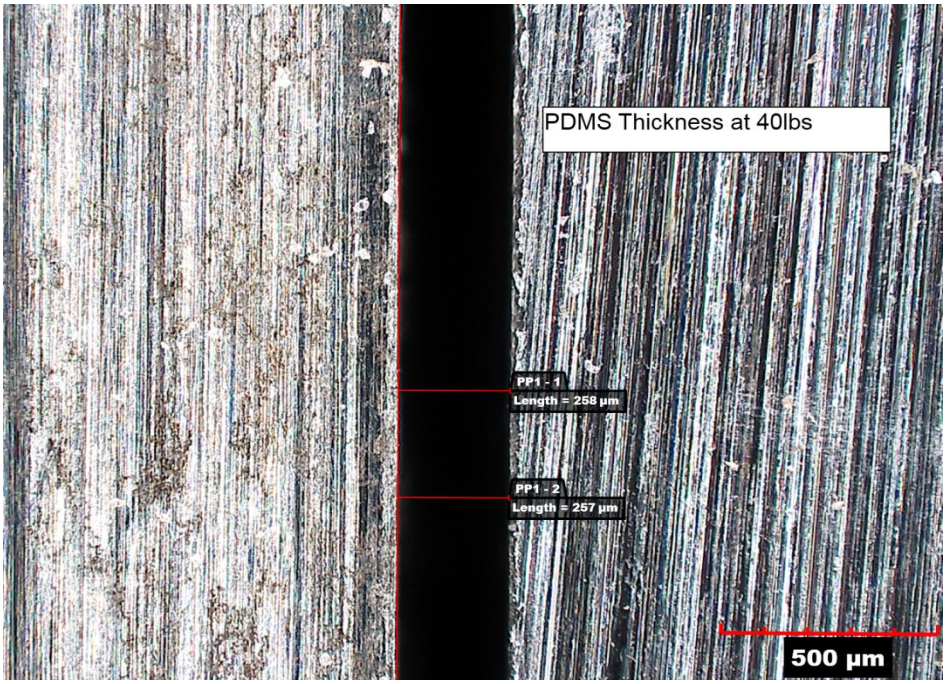

Figure C. Compressed thickness at various applied load (e) 40lbs (cont.).

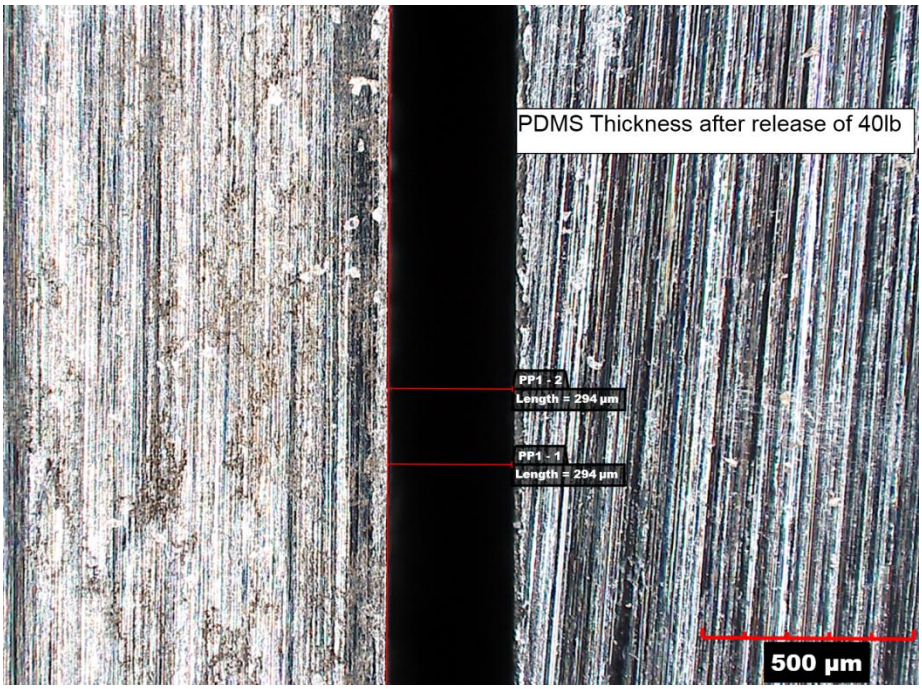

Figure C. Compressed thickness at various applied load (f) shows shape memory retention after 40lbs was removed (cont.).

APPENDIX D.

PROCEDURE FOR BONDING PDMS TO GLASS

Cured PDMS circular piece was cleaned using ultasonication in ethanol for 5 minutes to get rid of any surface contaminants viz. oil and dust and the bioglass discs were cleaned using compressed air. Following that both the PDMS and the bioglass (its polished surface faced up) were dry etched using Reactive Ion Etching using PE-200 SERIES PLASMA SYSTEM. Oxygen plasma at 60 W power, 120 mTorr pressure for 30 seconds. Thereafter, the PDMS sheet was carefully placed on the bioglass substrate to avoid air bubbles getting trapped in between the PDMS sheet and the glass. The resulting structure was kept on a hot plate at 60^{o} C and a slight pressure was applied for 10 minutes resulting in irreversible good bonding strength between PDMS and glass substrate.

The same process was applied to bond the second bioglass disc which will serve as second plate to the PDMS to complete making the capacitive device.

APPENDIX E.

PROCEDURE FOR DEVICE PACKAGING

Coaxial cables were connected to the trace area of the electrode using *Resinlab* silver paste (2 part mixture), cured for 6 hours at room temperature. It was followed by application of JB Weld which is a hard epoxy to provide further mechanical support. It was also cured for 6 hours at room temperature. Finally, RTV silicone was applied at that exposed area of coaxial cable connection to isolate it from solution and was left to cure overnight before measurements were started.

APPENDIX F.

PHOSPHATE BUFFER BODY FLUID PREPARATION

Phosphate Buffer Saline (PBS) was bought from Sigma Aldrich. The solution was prepared by mixing two entire pouches to 2 litres of de-ionized water. The resultant solution had a pH of 7.4. The solution was heated and maintained at 37 degree Celsius using hot plate throughout all the dissolution tests.

BIBLIOGRAPHY

[1] Irnich, W., Electronic security systems and active implantable medical devices, Journal of Pacing and Clinical Electrophysiology, 25(8), 1235-1258, 2002.

[2] Foster, K., Jaeger J., Ethical implications of implantable radiofrequency identification (RFID) tags in humans, The American Journal of Bioethics, 8(8), 44-48, 2008.

[3] Neufeld, E., S. Kuhn, G. Szekely, N. Kuster, Measurement, simulation and uncertainty assessment of implant heating during MRI, Physics in Medicine and Biology, 54(13), 4151-4169, 2009.

[4] Levine M, Adida B, Mandl K, Kohane I, Halamka J (2007) What Are the Benefits and Risks of Fitting Patients with Radiofrequency Identification Devices? PLoS Med 4(11): e322. doi:10.1371/journal.pmed.0040322.

[5] Lindner, P., V. Dragoi, S. Farrens, T. Glinsner, P. Hangweier, Advanced techniques for 3D devices in wafer-bonding processes, Solid State Technology, 47(6), 55-58, 2004.

[6] Rahaman, M.N., D. E. Day, S. Bal, Q. Fu, S. Jung, L. Bonewald, A. P. Tomsia, Bioactive glass in tissue engineering, Acta Biomaterialia, 7, 2355-2373, 2011.

[7] Biomechanics of the Lumbar Intervertebral Disk: A Review by Gail M Jensen Physical Therapy, 06/1980, Volume 60, Issue 6.

[8] M. A. Adams and P. Dolan. Spine biomechanics. Journal of Biomechanics 38(10), pp. 1972-1983. 2005.. DOI: 10.1016/j.jbiomech.2005.03.028.

[9] H. Wilke et al. New in vivo measurements of pressures in the intervertebral disc in daily life. Spine 24(8), pp. 755-762. 1999.. DOI: 10.1097/00007632-199904150-00005.

[10] W. Liang, C. Rüssel, D. E. Day, and G. Völksch, "Bioactive comparison of a borate, phosphate and silicate glass," *Journal of materials research*, vol. 21, no. 1, pp. 125-131, Jan. 2006. DOI: 10.1557/JMR.2006.0025.

[11] S. B. Jung and D. E. Day, "Conversion kinetics of silicate, borosilicate, and borate bioactive glasses to hydroxyapatite," *Physics and Chemistry of Glasses-European Journal of Glass Science and Technology Part B,* vol. 50, no. 2, pp. 85-88, Apr. 2009.

[12] M. Liu et al. Thickness-dependent mechanical properties of polydimethylsiloxane membranes. Journal of Micromechanics and Microengineering 19(3), pp. 035028. 2009. . DOI: 10.1088/0960-1317/19/3/035028.

[13] S. Zhou et al. Geometrical dimensions of the lower lumbar vertebrae analysis of data from digitised CT images. European Spine Journal 9(3), pp. 242-248. 2000.. DOI: 10.1007/s005860000140.

[14] Hong CH, Park JS, Jung KJ, Kim WJ. Measurement of the Normal Lumbar Intervertebral Disc Space Using Magnetic Resonance Imaging. *Asian Spine Journal*. 2010;4(1):1-6. doi:10.4184/asj.2010.4.1.1.

[15] http://www.elveflow.com/microfluidic-tutorials/soft-lithography-reviews-and-tutorials/introduction-in-soft-lithography/pdms-membrane-thickness-of-a-spin-coated-pdms-layer/. Last accessed 03/15/2017.

[16] Khanafer, K., Duprey, A., Schlicht, M. et al. Biomed Microdevices (2009) 11: 503. doi:10.1007/s10544-008-9256-6.

[17] I D Johnston, D K McCluskey, C K L Tan and M C Tracey, Mechanical characterization of bulk Sylgard 184 for microfluidics and microengineering, Journal of Micromechanics and Microengineering, Volume 24, Number 3.

[18] M. Liu et al. Thickness-dependent mechanical properties of polydimethylsiloxane membranes. Journal of Micromechanics and Microengineering 19(3), pp. 035028. 2009.. DOI: 10.1088/0960-1317/19/3/035028.

[19] Baxter, Larry K., "Capacitive Sensors," IEEE Press, Piscataway N.J., 1997.

[20] https://www.britannica.com/science/vertebral-column. Last accessed 03/14/2017.

[21] Huang, L. Dong and L. Wang. LC passive wireless sensors toward a wireless sensing platform: Status, prospects, and challenges. Journal of Microelectromechanical Systems 25(5), pp. 822-841. 2016. . DOI: 10.1109/JMEMS.2016.2602298.

VITA

Devdatt Chattopadhyay was born in Kolkata, India. He received his Bachelor of Technology degree from Heritage Institute of Science & Technology-Kolkata, India in Electronics & Communication Engineering (ECE) in 2013. He was also a summer research scholar at Microelectronics Center of New Jersey Institute of Technology, Newark USA in 2012 for an international student exchange program. He received his Master of Science in Electrical Engineering from Missouri University of Science and Technology-Rolla in May 2017.

He worked as Graduate Research Assistant in the Intelligent Microsystems Laboratory from 2014 to 2017 and a Graduate Teaching Assistant in the Dept. of Electrical Engineering from 2015 to 2017 at Missouri University of Science and Technology. His research interest included devices, sensors and semiconductors applications.